Modeling and Simulation of Biomass Gasification Integrated with Solid Oxide Fuel Cell System for Power Generation

Wajeha Tauqir

NUST-MS Energy System Engineering- 00000103863

Session 2016-18

Supervisor

Dr. Muhammad Zubair

U.S. Pakistan Center for Advanced Studies in Energy (USPCAS-E)

National University of Sciences and Technology (NUST)

H-12, Islamabad 44000, Pakistan

Modeling and Simulation of Biomass Gasification Integrated with Solid Oxide Fuel Cell System for Power Generation

Wajeha Tauqir

NUST-MS Energy System Engineering- 00000103863

Session 2016-18

Supervisor

Dr. Muhammad Zubair

A Thesis Submitted to the Centre for Energy Systems in partial fulfilment of the requirements for the degree of

MASTERS of Science in

ENERGY SYSTEMS ENGINEERING

U.S. Pakistan Center for Advanced Studies in Energy Systems (USPCAS-E)

National University of Sciences and Technology (NUST)

H-12, Islamabad 44000, Pakistan

August 2019

Thesis Acceptance Certificate

Certified that final copy of MS/MPhil thesis written by Miss Wajeha Tauqir (Registration No. 103863), of U.S Pakistan Center for Advanced Studies in Energy, has been vetted by undersigned, found complete in all respects as per NUST Statues/Regulations, is within the similarity indices limit and is accepted as partial fulfillment for the award of MS/MPhil degree. It is further certified that necessary amendments as pointed out by GEC members of the scholar have also been incorporated in the said thesis.

Signature: _____

Name of Supervisor: Dr. Muhammad Zubair

Date: _____

Signature (HoD): _____

Date: _____

Signature (Dean/Principal): _____

Date: _____

Certificate

This is to certify that work in this thesis has been carried out by **Ms. Wajeha Tauqir** and completed under my supervision in U.S. Pakistan Center for Advanced Studies in Energy (USPCAS-E), National University of Sciences and Technology, H-12, Islamabad, Pakistan.

Supervisor: _____

Dr. Muhammad Zubair
USPCAS-E
NUST, Islamabad

GEC member # 1: _____

Dr. Naseem Iqbal
USPCAS-E
NUST, Islamabad

GEC member # 2: _____

Dr. Rabia liaquat
USPCAS-E
NUST, Islamabad

GEC member # 3: _____

Dr. Iftikhar Ahmed Salarzai
SCME
NUST, Islamabad

HoD _____

Dr. Naseem Iqbal
USPCAS-E
NUST, Islamabad

Principal/ Dean _____

Dr. Zuhair S. Khan
USPCAS-E
NUST, Islamabad

Dedicated to

My Father(late) and Mother

For their love, support and encouragement

Abstract

In order to supply the electricity in off-grid rural areas, on-site energy generation technologies need to be developed. For this purpose, a detailed model of downdraft biomass gasifier integrated with Solid Oxide fuel cell(SOFC) the system was made and simulated to produce power of 120 kW. Aspen Plus software was used to model the system. It has inbuilt unit operation blocks which were used to model different stages and components of gasifier and fuel cell. Fortran coding was done to model different design specifications as well as power calculations. Gasifier produces a syngas which is used as a fuel for SOFC. SOFC then converts the chemical energy stored in fuel to electrical energy. Stack voltage is then calculated using the Nernst Voltage. Voltage losses were also calculated and subtracted from the Ideal Voltage. Both the models for gasifier and SOFC were validated using the data from the literature. Our models produced results very familiar with the results from the literature. Sensitivity analysis was done of following operating parameters for gasifier to check their effect on syngas composition and efficiency; gasification temperature, moisture content, and equivalence ratio. For SOFC sensitivity analysis was also done to check the effect of varying different parameters on Cell Voltage, Power output, Current density and efficiency of the system. Biomass flowrate, air utilization factor, and fuel utilization factor were the parameters analyzed. In order to check the performance of gasifier, cold gas efficiency and Low Heating Value of produced syngas were calculated. For SOFC's performance measurement, its gross, as well as net efficiencies, were calculated.

Keywords: *Biomass Gasification, Solid Oxide Fuel Cell, Aspen Plus, Modeling, Off-Grid System*

Table of Contents

List of Figures

List of Tables

List of Journal/Conference Papers

- Jyoti Prakasha, Daryn Roan, Wajeha Tauqir, Hassan Nazir, Majid Ali, Arunachala Kannana, "Off-grid solar thermal water heating system using phase-change materials: design, integration and real environment investigation" Applied Energy Volume 240, 15 April 2019, Pages 73-83 https://www.sciencedirect.com/science/article/pii/S0306261919303563

- Tauqir W, Zubair M, Nazir H. Parametric analysis of a steady state equilibrium-based biomass gasification model for syngas and biochar production and heat generation. Energy Conversion and Management 2019. Status: Under Review

Abbreviations

SOFC	Solid Oxide Fuel Cell
YSZ	Yttria stabilized zirconia
PR-BM	Peng Robinson equation of state with the Boston-Mathias alpha function
$\mathbf{V_N}$	Nernst Voltage
V_{ohm}	Ohmic Loss
V_{conc}	Concentration Loss
V_{act}	Activation Loss
$\eta_{SOFC,gross}$	SOFC Gross Efficiency
$\eta_{SOFC,net}$	SOFC Net Efficiency
LHV	Low Heating Value
CGE	Cold Gas Efficiency
ER	Equivalence Ratio
MC	Moisture Content
STCR	Steam to Carbon Ratio
UA	Air Utilization Factor
UF	Fuel Utilization Factor
ZJ	Current Density

Chapter 1: Introduction

1.1 Bioenergy Potential

Fossil fuels, have the largest share in today's world energy supply and will contribute to 80% of world's energy supply mix by 2040 if continued at the same pace [1], [2]. This scenario will lead to disastrous consequences in terms of environment because of greenhouse gas emissions associated with fossil fuel power plants. In order to avoid such situation in future renewables need to be incorporated more in energy mix. In recent year, two technologies; biomass gasification and fuel cells have gained a lot of attention in recent years.

Biomass is considered a renewable energy source. It has many advantages over fossil fuels. Energy potential of different biomass feedstock is huge, because of its vast availability and diversity. Biomass as an energy source, also mitigates a very common problem in most other renewables; like wind and solar, which is their dependency on weather and climate. Bioenergy is estimated to contribute to quarter and third of global energy supply mix by 2050 [3]. In terms of environmental affects, biomass has very small sulfur amount, produces very less amount of ash, and emit very less greenhouse gas emissions as compared to fossil fuels. Burning of biomass also produces very small amount of H_2S and other acidic gases which is the main source of acid rain. Thus, by incorporating biomass more and more in energy mix, will reduce the economic pressure caused by importing petroleum products for energy production [4] of biomass review.

Biomass Conversion technologies can be divided into four major categories which are [4];

Direct Combustion Processes

Produced energy can be used, cooking, heating, in industries for large scale processes, as well as electricity generation in thermal power plants.

Biochemical Processes

Processes involving anaerobic digestion and fermentation processes.

Agrochemical Processes

Such processes are those which employ mechanical methods, like extraction of rapeseed oil from rapeseed.

Thermochemical processes

Such processes are those which involve using heat energy to increase chemical transformation of biomass into energy and other chemical products. Examples of thermochemical processes include; pyrolysis, gasification, and direct liquefaction. Biomass gasification to produce syngas (mixture of CO and H_2) is one of the major application of gasification process. Produced syngas can be used in synthesis of various other chemicals like, Fischer troph fuels and ammonia [5]. Syngas can also be used as a fuel in internal combustion engines and fuel cells [6].

1.2 Fuel Cell's Electricity Generation Potential

Fuel Cell converts chemical energy into electrical by electrochemically combining fuel with an oxidant. It has many advantages. It produces very low NO_X and CO_2 emissions, has high conversion efficiency, and environmental acceptability. Application of fuel cells in power generation applications have gained a lot of popularity among the researchers and seem to be very promising option to provide clean electricity in future [7].

Solid Oxide Fuel Cell among the fuel cells, is one of the most efficient and environmental friendly technology available for power generation. It utilizes syngas, methane, hydrogen and other renewable fuels for power generation. Pilot scale SOFC systems have been developed and demonstrated in US, Japan, and different areas of Europe. SOFC's are also being developed for residential, industrial, transportation and military applications [8]. They operate at high temperatures (around 600-1000 ^oC). High temperatures, allow internal reforming of methane, thus, variety of fuels can be used as fuel for SOFC. SOFC being fuel flexible allow biomass derived syngas to be used as fuel.

Such systems including integration of biomass gasifier with solid oxide fuel cell, can be a very suitable option to supply electricity to rural areas, where no transmission grid is present.

1.3 Scope of the Work

Biomass is one of the most cost effective and widely available energy resource in Pakistan. In order to meet the shortfall of energy in Pakistan, there is a need to tap in all the available resources. For this reason, new energy conversion systems need to be evaluated and optimized. There is a lot of research and work done recently on the hybridization of biomass gasification and solid oxide fuel cell systems. These systems so far seem to be very promising option for the cogeneration of heat and electricity, and their conversion efficiencies are greater than 40%. These carbon neutral energy generation systems can be a very suitable option to provide electricity to rural areas of Pakistan.

Summary

This chapter, gives a brief overview of current status of bioenergy in world. Benefits of bioenergy and its applications. Also, the enormous potential fuel cells have energy generation sector were also explained.

References

[1] U. Energy Information Administration, “International Energy Outlook 2013 with Projections to 2040,” 2013.

[2] “World Energy Outlook 2013 Factsheet. How will global energy markets evolve to 2035?,” 2013.

[3] A. Bauen *et al.*, “Bioenergy: a sustainable and reliable energy source. A review of status and prospects.,” *Bioenergy a Sustain. Reliab. energy source. A Rev. status Prospect.*, 2009.

[4] A. Demirbaş, “Biomass resource facilities and biomass conversion processing for fuels and chemicals,” *Energy Convers. Manag.*, vol. 42, no. 11, pp. 1357–1378, Jul. 2001.

[5] P. Lv, Z. Yuan, C. Wu, L. Ma, Y. Chen, and N. Tsubaki, “Bio-syngas production from biomass catalytic gasification,” *Energy Convers. Manag.*, vol. 48, no. 4, pp. 1132–1139, Apr. 2007.

[6] M. Asadullah, S. Ito, K. Kunimori, M. Yamada, and K. Tomishige, “Biomass Gasification to Hydrogen and Syngas at Low Temperature: Novel Catalytic System Using Fluidized-Bed Reactor,” *J. Catal.*, vol. 208, no. 2, pp. 255–259, Jun. 2002.

[7] S. Samuelsen, “Fuel Cell/Gas Turbine Hybrid Systems,” 2004.

[8] N. Laosiripojana, W. Wiyaratn, W. Kiatkittipong, A. Arpornwichanop, A. Soottitantawat, and S. Assabumrungrat, “Reviews on Solid Oxide Fuel Cell Technology,” *Eng. J.*, vol. 13, no. 1, pp. 65–84, Feb. 2009.

Chapter 2: Literature Review

This chapter briefly explains the important principles of gasification and working of fuel cell system.

2.1 Biomass Gasification

Gasification is one of the most effective and common method of producing syngas (H_2 +CO) from biomass. Gasification can be done for different types of feedstock, e.g. biomass, coal, industrial waste, natural gas and petroleum [9]. Biomass include any organic material which comes from animals or plants. Biomass can be majorly divided into two main groups; Virgin and waste biomass [10].

Table 1. Classification of Biomass Feedstock

Virgin Biomass	Woody	Trees, vines, shrubs, bushes etc.
	Herbaceous	Plants that at the end of growing season
	Energy Crops	Willow, poplar, switch grass etc.
Waste Biomass	Agricultural waste	Livestock and manures, Agricultural crop residue
	Municipal waste	Municipal solid waste, Biosolids, sewage, Landfill gas
	Industrial waste	Black liquor, Demolition wood, Waste oil or fat
	Forestry waste	Bark, leaves, floor residues

2.1.1 Gasification Principle

Biomass Gasification is the thermochemical conversion of solid/liquid fuels into gaseous/vapours and solid products. The vapour fraction of the product stream mostly called syngas consist of CO, H_2, CH_4, light hydrocarbons (such as ethane, propane) and heavier hydrocarbons (such as tar). Syngas produced from gasification mostly have high low heating value (4-13 MJ/Nm^3) and can be used for power generation. It also contains undesirable gases (such as N_2, H_2S, HCl etc.)[11]–[13]. The solid portion is called char which consist of unconverted organic fraction and inert materials in the fed biomass. LHV of char varies from 25-30 MJ/kg [14]. The amount of vapour and liquid fractions as well as their compositions and heating values both depend on the biomass feedstock, operating conditions, and gasification technology.

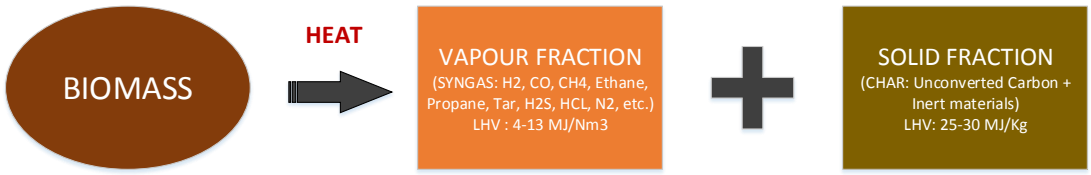

Figure 1. Biomass Gasification Principle

2.1.2 Gasification Process

Gasification process consists of four major steps;

1. Drying,
2. Pyrolysis,
3. Oxidation, and
4. Reduction

Of all four steps only one, oxidation is exothermic, while the other three are endothermic. Oxidation step is also responsible to provide heat energy required by other endothermic processes [15], [16].

2.1.2.1 Drying

First step of gasification is drying in which the moisture content of biomass feedstock is reduced to certain amount by supplying heat. Higher amounts of moisture in feedstock results in more energy loss as well as lower syngas heating value. Amount of required moisture content in feedstock for gasification varies from 5-35% and depends upon the nature of feedstock. Drying of biomass feedstock is mostly achieved at around 100-150 ^{O}C [17]–[21]

$$\text{Moist Feedstock} + \text{Heat} \rightarrow \text{Dry Feedstock} + H_2O \qquad (1)$$

2.1.2.2 Pyrolysis

Pyrolysis process involves the thermochemical decomposition of the carbonaceous material into lower molecular weight compounds in the absence of oxygen/ air. The product consists of the solid liquid, and gaseous fractions. The solid fraction for fixed bed gasifiers, range from 20-25 wt% and have high heating value and carbon content. This fraction, contains inert materials(ashes), as well as char [22]–[25]. Liquid fraction consists of complex organic compounds called tar which are condensable at relatively low temperature. For downdraft gasifiers, liquid fraction is < 1wt% [25]–[27]. Gaseous portion constitutes the major portion of pyrolysis product, 70-90 wt% for downdraft gasifier. It includes gases which are incondensable at ambient temperature. It consists mainly of H_2, CO, CO_2, CH_4, other hydrocarbons, and minor quantity of inert and acid gases. This step takes place at temperature range of 250-700 ^{O}C [25], [26], [28]. Reactions taking place below 300^{o}C are endothermic while those above 300 ^{o}C are exothermic. Thus, for high temperature processes external heating is required to maximize the gaseous fraction[18]–[21]**.**

$$\text{Dry Feedstock} + \text{Heat} \rightarrow \text{Char} + \text{Volatiles} \qquad (2)$$

2.1.2.3 Partial Oxidation

At this stage, heterogeneous reactions take place between solid carbonaceous fuel and oxygen to produces carbon dioxide and a substantial amount of heat. Oxygen less than the stoichiometric requirement is supplied to ensure partial oxidation. Hydrogen also react with oxygen to form H_2O [18]–[21]**.**

Main oxidation reactions are;

$$C + O_2 \rightarrow CO_2 + 406 \text{ MJ/kg. mole} \quad (3)$$

$$2\ H_2 + O_2 \rightarrow 2\ H_2O + 242 \text{ MJ/kg mole} \quad (4)$$

Nitrogen is also present in the product gas if oxidation is performed with air other than O_2. Heat produced by these reactions can be used in the drying, pyrolysis as well as the reduction step.

2.1.2.4 Reduction

In this zone, a number of chemical reactions take place at relatively high temperatures to produce high heating value syngas (mainly CO and H_2). These reactions convert sensible heat of pyrolysis gas into chemical energy of producer gas. Main reactions, in the reduction zone are;

$$C + CO_2 \rightarrow 2\ CO - 172.6 \text{ MJ/kg. mole (Boudourd reaction)} \quad (5)$$

$$C + H_2O \rightarrow CO + H_2 - 131.4 \text{ MJ/kg. mole (Water gas reaction)} \quad (6)$$

$$CO + H_2O \rightarrow CO_2 + H_2 + 42.3 \text{ MJ/kg. mole (Water gas shift reaction)} \quad (7)$$

$$C + 2\ H_2 \rightarrow CH_4 + 75 \text{ MJ/kg. mole (Methanation reaction)} \quad (8)$$

The first two of these reactions are endothermic and the other two water gas shift and methanation are exothermic. Reaction, 7 and 8 are favoured at high temperatures while 5 and 6 are favoured at low temperatures. Since reaction 5 and 6 contribute more at high temperatures, they make the reduction step endothermic. Therefore, the temperature at which reduction takes place plays a key role in determining the composition heating value of syngas. Typical temperature range for the reduction step is 800-1100 ^{O}C.

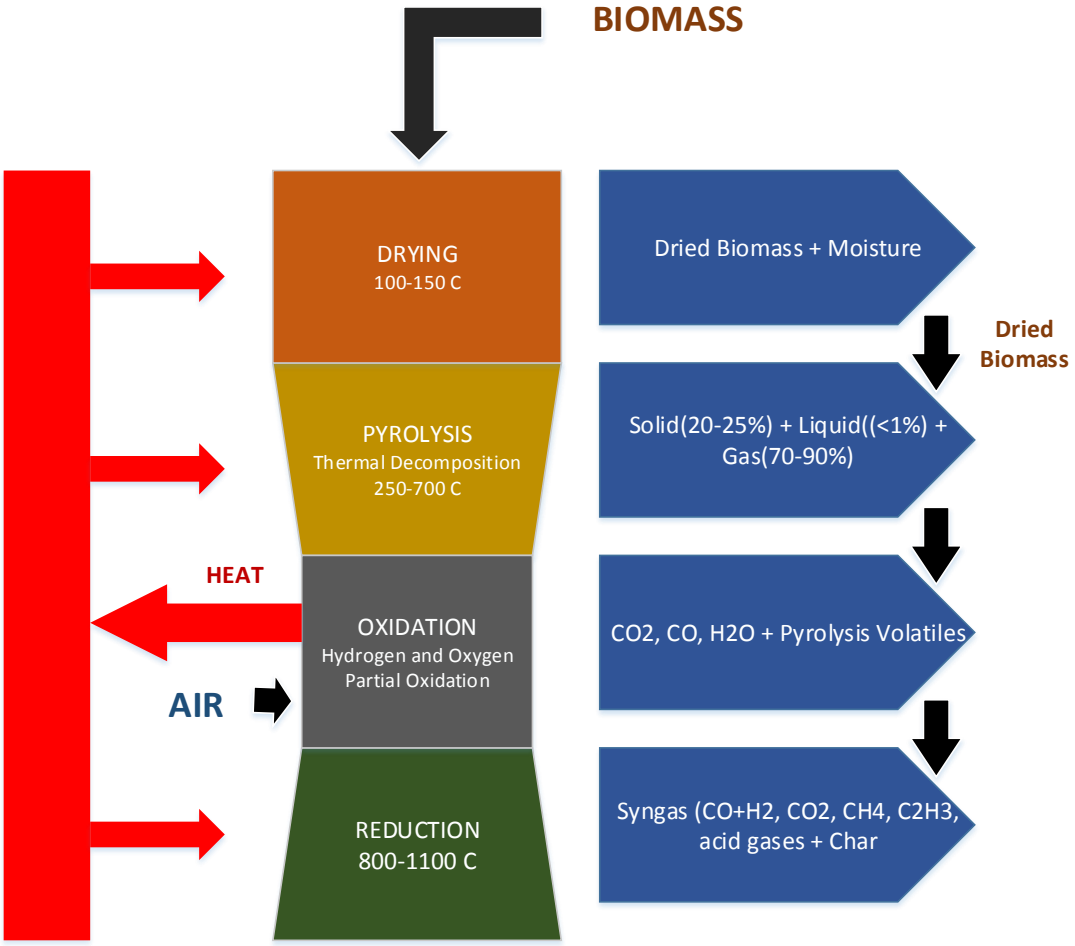

Figure 2. Downdraft Biomass Gasification Process

2.2 Fuel Cells

Fuel cells are electrochemical devices which convert chemical energy directly into electrical energy[29], [30]. Hydrogen contains significant amount of chemical energy as compared to battery materials hence can be used as a substitute for conventional energy generation in various applications.

Fuel cells can be applied for small energy applications, like 1W to 10kW, in personal electronic devices e.g. cell phones and computers. They can also be employed in 1-100kW range applications e.g. transportation. Also for very high range applications, 1-10 MW, like power systems for electricity generation[31], [32].

Fuel cell technology can be used to supply electricity in rural areas; where electricity grid cannot reach or it gets too costly to lay the wiring for transferring electricity. Also, fuel cell can also aid in conventional power generation stations, and distributed systems by acting as their source of energy. A comparison between fuel cells and other power generation technologies is shown in table 1[29], [31], [33], [34];

Table 2. Comparison Between Fuel cells and other Power generation Technologies

	Reciprocating engine: diesel	Turbine generator	Photovoltaic	Wind turbine	Fuel cells
Capacity range	500 kW–50 MW	500 kW–5 MW	1 kW–1 MW	10 kW–1 MW	200 kW–2 MW
Efficiency	35%	29–42%	6–19%	25%	40–85%
Capital cost ($/kW)	200–350	450–870	6600	1000	1500–3000
O & M cost ($/kW)	0.005–0.015	0.005–0.0065	0.001–0.004	0.01	0.0019–0.0153

According to this comparison fuel cells show highest conversion efficiency. Although, its capital cost is high, but due to its simple operation and design it has low maintenance cost. Also, since it uses hydrogen as an energy source they are environmentally clean energy generation systems [35]–[39]. Other than the high

capital cost, fuel cell technology has few more shortcomings, for example, low per density per volume, less durability and accessibility, also the impurities in gas stream decreases their life. Still, very positive developments have been made in fuel cell technology in the past few years, and researchers are very keen to make this technology more reliable and practical.

2.2.1 Working Principle of Fuel Cells

In fuel cells oxygen and hydrogen undergo electrochemical reactions to generate electricity and heat. Water is formed as a by-product. Fuel cells have different designs but they all operate at the same basic principle. The main difference in different fuel cell types, is their electrolyte. Electrolyte allows protons to move between two sides of fuel cells. Thus, most of the properties of the fuel cell depends on the chemical characteristics of electrolyte used in them [40].

Equation 9 and 10 shows the basic reaction in fuel cell.

$$2\ H_2\ (g) + O_2\ (g) \rightarrow 2\ H_2O + \text{energy} \qquad (9)$$

$$\text{Hydrogen} + \text{oxygen} \rightarrow \text{water} + (\text{electrical power} + \text{heat}) \qquad (10)$$

Major parts of fuel cell include; anode, cathode, external circuit and electrolyte. At anode, catalyst cause, fuel (hydrogen) to undergo oxidation and produce proton and electron. These generated protons move through electrolyte to cathode. Electrons travel through the external circuit from anode to cathode where it reduces the oxygen molecules. At cathode, both protons and oxygen ions react to form water. Travel of electrons through the external circuit from anode to cathode generates current. Either oxide or proton pass through electrolyte depending on the chemical properties of the electrolyte. Electrolyte do not allow electrons to flow through it restricting their transport through external circuit only [41]. Amount of current produced from fuel cells is very small because of the very small contact area between electrolyte, electrodes and gas streams. Also the distance between electrodes also affect the travel time of protons and generation of current. Thus, for more electrolyte and gas penetration in electrodes to increase fuel cell's efficiency, thin layer of electrolyte with porous electrodes is considered.

Different fuel cells have different electrochemical reactions between hydrogen and oxygen.

The reactions occurring in acid electrolyte fuel cell are given by equations 11 and 12.

$$\text{Anode: } 2\,H_2 \rightarrow 4H^+ + 4e- \qquad (11)$$

$$\text{Cathode: } O_2 + 4e^- + 4H^+ \rightarrow 2\,H_2O \qquad (12)$$

These acid electrolytes only allow H^+ ions to pass through it and thus are called proton exchange membranes. If electrons were to pass through electrolyte, than electrical current will be lost in the process [29].

2.2.2 Types of Fuel Cells

Fuel cells, are classified into six groups depending on their fuel and electrolyte type [31]:

1. Alkaline fuel cell (AFC)
2. Phosphoric acid fuel cell (PAFC)
3. Solid oxide fuel cell (SOFC)
4. Molten carbonate fuel cell (MCFC)
5. Proton exchange membrane fuel cell (PEMFC)
6. Direct methanol fuel cell (DMFC)

Table below gives a comparison of different fuel cell technologies; [29], [42]–[44];

Table 3. Comparison of Different Fuel cell Technologies

Fuel Cell Type	Common Electrolyte	Anode reaction	Cathode reaction	Operating Temperature (◦C)	Fuel	Oxidant	Cell Voltage	System Output (kW)	Electrical Efficiency (%)	Combines Heat and Power (CHP) Efficiency	Applications	Advantages
AFC	Aqueous solution of potassium hydroxide soaked in a matrix	$2H_2 + 4OH^- \rightarrow 4H_2O + 4e^-$	$O_2 + 2H_2O + 4e^- \rightarrow 4OH^-$	90–100	Pure H_2	O_2 in air	1.0	10–100	60	>80	Military Space	Cathode reaction faster in alkaline electrolyte, leads to higher performance
PAFC	Liquid phosphoric acid soaked in a matrix	$2\ H_2 \rightarrow 4\ H^+ + 4\ e^-$	$O_2 + 4\ H^+ + 4e^- \rightarrow H_2O$	150–200	Pure H_2	O_2 in air	1.1	50–1000	>40	>85	Distributed generation	Higher overall efficiency with CHP Increased tolerance to impurities in hydrogen
SOFC	Yttria stabilized zirconie	O_2^- (S) + H_2 (g)→ H_2O (g) +2 e^-	1/2 O_2 (g) + 2e^- →O_2^-(s)	600–1000	H_2, CO, CH_4, other	O_2 in air	0.8–1.0	<1–3000	35–43	<90	Auxiliary power Electric utility Large distributed generation	High efficiency Fuel flexibility Can use a variety of catalysts Solid electrolyte reduces electrolye management problems Suitable for CHP Hybrid/GT cycle
MCFC	Liquid solution of lithium, sodium, and/or potassium carbonates, soaked in a matrix	$H_2O + CO_2^{-3} \rightarrow H_2O + CO_2 + 2\ e^-$	$1/2\ O_2 + CO_2 + 2e^- \rightarrow CO_2^{-3}$	600–700	H_2, CO, CH_4, other	O_2 in air	0.7–1.0	<1–1000	45–47	>80	Electric utility Large distributed generation	High efficiency Fuel flexibility Can use a variety of catalysts Suitable for CHP
PEMFC	Solid organic polymer poly-perfluorosulfonic acid	H_2 (g)→2 H^+ +2 e^-	$1/2O_2$ (g) + $2H^+ + 2e- \rightarrow H_2O$	50–100	Pure H_2	O_2 in air	1.1	<1–250	53–58	70–90	Backup power Portable power Small distributed generation Specialty vehicle Transportation	Solid electrolyte reduces corrosion & electrolyte management problems Low temperature Quick start-up
DMFC	Solid polymer membrane	$CH_3OH + H_2O \rightarrow CO_2 + 6H^+ + 6e^-$	$3/2O_2 + 6e^- + 6H^+ \rightarrow 3H_2O$	60–200	CH_3OH	O_2 in air	0.2–0.4	0.001–100	40	80	Replace batteries in mobiles; computers and other portable devices	Reduced cost due to absence of fuel reformer

2.2.3 Solid Oxide Fuel Cells

Solid oxide fuel cells (SOFC) are characterized by their high operating temperatures and metallic solid oxide or ceramic electrolyte.

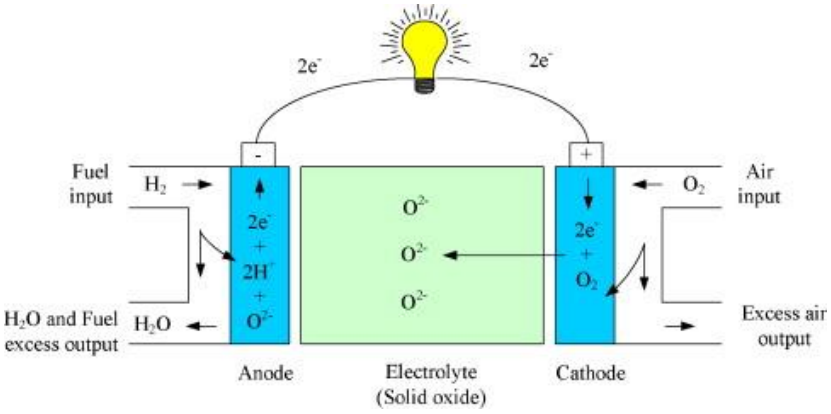

Figure 3. Working Principle of SOFC [45]

SOFC'S instead of using only hydrogen as an energy source, use a mixture of carbon monoxide and hydrogen which is formed as a result of the internal reforming of hydro carbonaceous fuel and oxidant in fuel cell [41]. For electrolyte, Yttria stabilized zirconia (YSZ) is mostly used because of their pure ionic conductivity and chemical and thermal stablity [46], [47].

Fuel is supplied to anode while oxidant (air/pure oxygen) is supplied to cathode. Oxygen is oxidized at cathode and fuel is reduced at anode, both at around 1000 °C. Porous anode is used to make the fuel and products movement easier [48]–[50]

Oxidation and Reduction reactions occurring in SOFC's are given in equation 13 and 14.

$$\text{Oxidation: } (1/2)\, O_2\,(g) + 2e^- \rightarrow O^{2-}(s) \qquad (13)$$

$$\text{Reduction: } O^{2-}\,(s) + H_2\,(g) \rightarrow H_2O\,(g) + 2e^- \qquad (14)$$

SOFC are majorly employed in distributed power generation, capable of generating power up to hundreds of megawatts. The heat generated as a by-product can also be used in gas turbines thus producing more electricity and increasing the combined heating and power efficiency to 70-80 %. SOFC's are fuel adaptable and

modular with low greenhouse gas emissions. They are extremely suitable for areas where the public grid does not supply electricity.

However, work needs to be done to manage their long start-up and cooling times, as well as several mechanical and chemical stability issues also arise due to their high operating temperatures. Researchers have explained various solutions to lower their operating temperatures and sustainable counter measures for SOFC [47]–[49], [51], [52].

Summary

In this section basic principle of biomass gasification was explained, together with the detailed chemistry of different stages of biomass gasification. Different stages of gasification include; Drying, Pyrolysis, Oxidation, and Reduction. In the second part of this section, working principle of fuel cells is explained. Fuel cells are categorized based on the types of electrolyte. Solid Oxide fuel cell is explained in detail, since it will be modelled in this study.

References

[9] A. A. Ahmad, N. A. Zawawi, F. H. Kasim, A. Inayat, and A. Khasri, "Assessing the gasification performance of biomass: A review on biomass gasification process conditions, optimization and economic evaluation," *Renew. Sustain. Energy Rev.*, vol. 53, pp. 1333–1347, 2016.

[10] A. Bhavanam and R. C. Sastry, "Biomass Gasification Processes in Downdraft Fixed Bed Reactors : A Review," *Int. J. Chem. Eng. Appl.*, vol. 2, no. 6, pp. 425–433, 2011.

[11] B. Liu, "Comparative study of fluidized-bed and fixed-bed reactor for syngas methanation over Ni-W / TiO 2 -SiO 2 catalyst," *J. Energy Chem.*, vol. 22, no. 5, pp. 740–746, 2013.

[12] K. Qian *et al.*, "Effects of Biomass Feedstocks and Gasification Conditions on the Physiochemical Properties of Char," pp. 3972–3986, 2013.

[13] Y. Wu, W. Yang, and W. Blasiak, "Energy and Exergy Analysis of High Temperature Agent Gasification of Biomass," pp. 2107–2122, 2014.

[14] C. Bulmau, C. Marculescu, A. Badea, and T. Apostol, "Pyrolysis parameters influencing the bio-char generation from wooden biomass," vol. 72, 2010.

[15] R. Rauch, J. Hrbek, and H. Hofbauer, "Biomass gasification for synthesis gas production and applications of the syngas," *Wiley Interdiscip. Rev. Energy Environ.*, vol. 3, no. 4, pp. 343–362, Jul. 2014.

[16] J. Zhang, W. Li, and Z. Gan, "Effect of supercritical water on the stability and activity of alkaline carbonate catalysts in coal gasification," *J. Energy Chem.*, vol. 22, no. 3, pp. 459–467, 2013.

[17] P. C. Faaij, H. Den Uil, C. N. Hamelinck, and H. Boerrigter, "Production of FT transportation fuels from biomass ; technical options , process analysis and optimisation , and development potential," vol. 29, pp. 1743–1771, 2004.

[18] M. A. Chawdhury and K. Mahkamov, "Development of a Small Downdraft

Biomass Gasifier for Developing Countries," *J. Sci. Res.*, vol. 3, no. 1, p. 51, Dec. 2010.

[19] A. Kumar, D. Jones, and M. Hanna, "Thermochemical Biomass Gasification: A Review of the Current Status of the Technology," *Energies*, vol. 2, no. 3, pp. 556–581, Jul. 2009.

[20] T. Srivastava, "Renewable Energy (Gasification)," *Adv. Electron. Electr. Eng.*, vol. 3, no. 9, pp. 1243–1250, 2013.

[21] I. Conference, S. Energy, and A. G. Growth, "e r ı e r," no. November, pp. 116–119, 2014.

[22] X. T. Li, J. R. Grace, C. J. Lim, A. P. Watkinson, H. P. Chen, and J. R. Kim, "Biomass gasiÿcation in a circulating uidized bed," vol. 26, pp. 171–193, 2004.

[23] P. . M. Lv, Z. h. Xiong, J. Chang, C. Z. Wu, Y. Chen, and J. X. Zhu, "An experimental study on biomass air – steam gasification in a fluidized bed," vol. 95, pp. 95–101, 2004.

[24] A. Go, R. Arjona, and P. Ollero, "Pilot-Plant Gasification of Olive Stone :," pp. 598–605, 2005.

[25] C. J. Roos, "Clean Heat and Power Using Biomass Gasification for Industrial and Agricultural Projects," vol. 3165, no. February, 2010.

[26] J. C. Schmid, U. Wolfesberger, S. Koppatz, C. Pfeifer, and H. Hofbauer, "Variation of Feedstock in a Dual Fluidized Bed Steam Gasifier — Influence on Product Gas , Tar Content , and Composition," vol. 31, no. 2, pp. 205–215, 2012.

[27] D. L. Carpenter, S. P. Deutch, and R. J. French, "Quantitative Measurement of Biomass Gasifier Tars Using a Molecular-Beam Mass Spectrometer : Comparison with Traditional Impinger Sampling," no. 3, pp. 3036–3043, 2007.

[28] M. Widyawati, T. L. Church, N. H. Florin, and A. T. Harris, "Hydrogen synthesis from biomass pyrolysis with in situ carbon dioxide capture using

calcium oxide," *Int. J. Hydrogen Energy*, vol. 36, no. 8, pp. 4800–4813, 2011.

[29] J. Larminie and A. Dicks, "Fuel Cell Systems Explained Second Edition."

[30] W. Vielstich, A. Lamm, H. A. (Hubert A. Gasteiger, and H. Yokokawa, *Handbook of fuel cells : fundamentals, technology, and applications*. Wiley, 2003.

[31] A. Kirubakaran, S. Jain, and R. K. Nema, "A review on fuel cell technologies and power electronic interface," *Renew. Sustain. Energy Rev.*, vol. 13, no. 9, pp. 2430–2440, Dec. 2009.

[32] A. Boudghene Stambouli and E. Traversa, "Fuel cells, an alternative to standard sources of energy," *Renew. Sustain. Energy Rev.*, vol. 6, no. 3, pp. 295–304, Sep. 2002.

[33] G. Nahar and K. Kendall, "Biodiesel formulations as fuel for internally reforming solid oxide fuel cell," *Fuel Process. Technol.*, vol. 92, no. 7, pp. 1345–1354, Jul. 2011.

[34] "What Are Batteries, Fuel Cells, and Supercapacitors?," 2004.

[35] X. Zhang and Z. Shen, "Carbon fiber paper for fuel cell electrode," *Fuel*, vol. 81, no. 17, pp. 2199–2201, Dec. 2002.

[36] A. Larrosa-Guerrero, K. Scott, I. M. Head, F. Mateo, A. Ginesta, and C. Godinez, "Effect of temperature on the performance of microbial fuel cells," *Fuel*, vol. 89, no. 12, pp. 3985–3994, Dec. 2010.

[37] H. Xu, L. Kong, and X. Wen, "Fuel Cell Power System and High Power DC–DC converter," *IEEE Trans. Power Electron.*, vol. 19, no. 5, pp. 1250–1255, Sep. 2004.

[38] C. Rayment and S. Sherwin, "Introduction to Fuel Cell Technology," 2003.

[39] W. R. Grove, "XXIV. *On voltaic series and the combination of gases by platinum*," *London, Edinburgh, Dublin Philos. Mag. J. Sci.*, vol. 14, no. 86–87, pp. 127–130, Feb. 1839.

[40] B. Cook, “Introduction to fuel cells and hydrogen technology,” *Eng. Sci. Educ. J.*, vol. 11, no. 6, pp. 205–216, Dec. 2002.

[41] R. M. Ormerod, “Solid oxide fuel cells,” 2003.

[42] A. B. Stambouli, “Fuel cells: The expectations for an environmental-friendly and sustainable source of energy,” *Renew. Sustain. Energy Rev.*, vol. 15, no. 9, pp. 4507–4520, Dec. 2011.

[43] O. Z. Sharaf and M. F. Orhan, “An overview of fuel cell technology: Fundamentals and applications,” *Renew. Sustain. Energy Rev.*, vol. 32, pp. 810–853, Apr. 2014.

[44] Z. Ud Din and Z. A. Zainal, “Biomass integrated gasification-SOFC systems: Technology overview,” *Renew. Sustain. Energy Rev.*, vol. 53, pp. 1356–1376, 2016.

[45] J. M. Andújar and F. Segura, “Fuel cells: History and updating. A walk along two centuries,” *Renew. Sustain. Energy Rev.*, vol. 13, no. 9, pp. 2309–2322, Dec. 2009.

[46] J. Will, A. Mitterdorfer, C. Kleinlogel, D. Perednis, and L. . Gauckler, “Fabrication of thin electrolytes for second-generation solid oxide fuel cells,” *Solid State Ionics*, vol. 131, no. 1–2, pp. 79–96, Jun. 2000.

[47] S. . Singhal, “Advances in solid oxide fuel cell technology,” *Solid State Ionics*, vol. 135, no. 1–4, pp. 305–313, Nov. 2000.

[48] K. Tanaka, C. Wen, and K. Yamada, “Design and evaluation of combined cycle system with solid oxide fuel cell and gas turbine,” *Fuel*, vol. 79, no. 12, pp. 1493–1507, Oct. 2000.

[49] M. Sahibzada, B. C. H. Steele, D. Barth, R. A. Rudkin, and I. S. Metcalfe, “Operation of solid oxide fuel cells at reduced temperatures,” *Fuel*, vol. 78, no. 6, pp. 639–643, May 1999.

[50] “Solid oxide fuel cell, Wikipedia.” 2015.

[51] T. Hibino, A. Hashimoto, T. Inoue, J. Tokuno, S. Yoshida, and M. Sano, “A low-operating-temperature solid oxide fuel cell in hydrocarbon-Air mixtures,” *Science*, vol. 288, no. 5473, pp. 2031–3, Jun. 2000.

[52] “Fuel Cells - Wikipedia,” 2019. [Online]. Available: https://en.wikipedia.org/wiki/Fuel_cell. [Accessed: 27-Apr-2019].

Chapter 3: Design and Modeling of Gasifier and Fuel Cell

This chapter briefly explains the design and modeling of gasifier and fuel cell.

3.1 Biomass Gasification Modeling

In this thesis, biomass gasification process is modelled using Aspen Plus simulator. Aspen Plus allows to simulate chemical engineering processes using inbuilt different process models. First of all, process flowsheet is made built using its unit operation blocks. Their property method, and initial and operating conditions are specified.

Peng Robinson equation of state with the Boston-Mathias alpha function (PR-BM), was specified as the property method to calculate thermodynamic properties of the components [53]. PR-BM is used for processes involving, nonpolar and mildly polar mixtures such as light gases and hydrocarbons. Units were set to METSOLIDS, which uses metric system units. All the components in the process were than specified as conventional components except for Biomass and Ash which were specified as Non-Conventional. For NC components, enthalpy calculation model was set to HCOALGEN, and density to DCOALIGT [54]. Both of these methods, perform calculations based on the ULTIMATE, PROXIMATE, and SULFANAL analysis when all four option codes are set to 1. Option codes define how the heat of combustion, the standard heat of formation, the heat capacity, and the enthalpy will be calculated. For Biomass first code was changed to 6, to specify heat of combustion of biomass. In the simulation mode, stream class was set to MIXCINC. It is used when both conventional and nonconventional solids are present, but without particle size distribution. Here MIX is for mixed substream, CI for CISOLID, and NC for nonconventional components.

3.1.1 Flowsheet Development

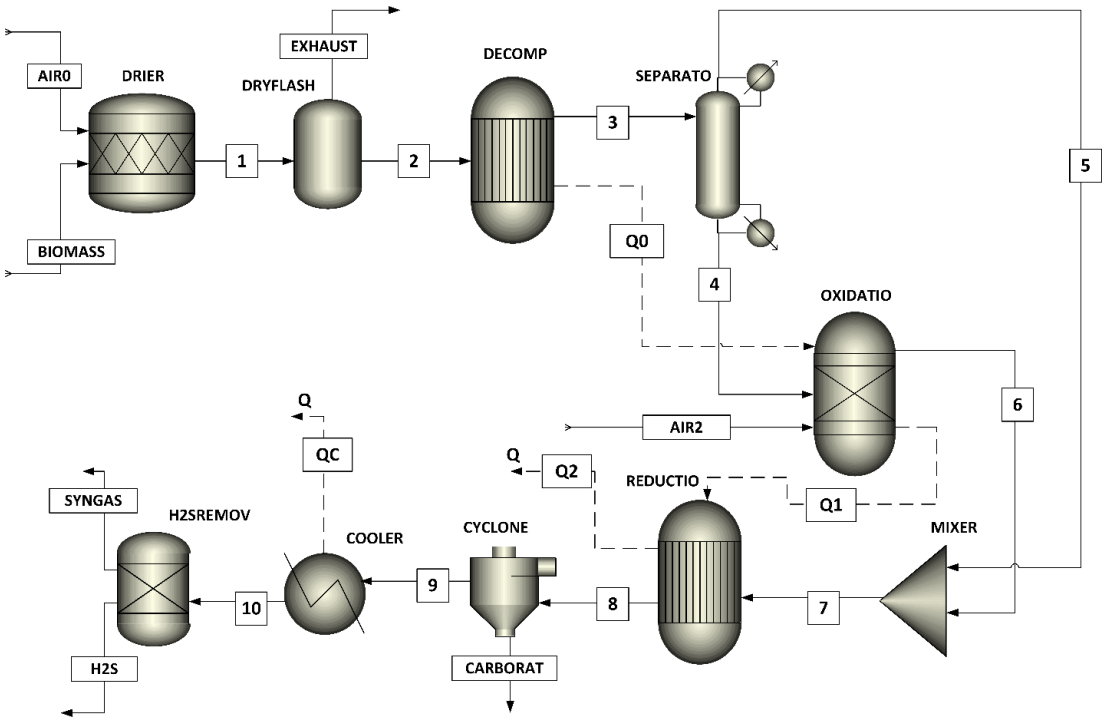

Figure 4. Aspen Plus Biomass Gasification Flowsheet

Main Assumptions:

1. The whole process is isothermal and steady-state
2. Char consists only of carbon and ash
3. Tar and other heavy hydrocarbons are not considered
4. Blocks are considered zero-dimensional, characterized by uniform temperature and perfect mixing
5. Residence time is enough to reach equilibrium in the R-Gibbs block
6. Biomass particles size distribution is not considered and they are assumed to spherical and not affected during the course of reactions

"Drier" block is used to simulate the drying of biomass feedstock. Rstoic unit operation block is used for this process. BIOMASS stream defined as NC stream with proxanal, ultanal, and sulfanal attributes added to it was introduced in the Drier block. Air at atmospheric pressure and elevated temperature was entered in the "Drier" block through the stream "AIR0" to provide heat for the drying process. Rstoic block is used to convert a portion of biomass into water. The following reaction is specified in the Rstoic block to model the conversion process.

$$\text{biomass (wet)} \rightarrow 0.0555084\ H_2O \qquad (15)$$

According to it 1 mole of biomass reacts to form 0.0555084 moles of water. This general reaction is used because the modelled gasifier is to be used for different biomass feedstock. Fractional conversion of biomass was initially set to 0.2, which will be later set by a calculator block.

Drying the biomass will change the moisture value in the proximate analysis. Rest of the elements in proxanal, sulfanal and ultanal analysis are on dry basis, thus they will not be disturbed during the drying process. Thus, value for moisture in proxanal component attribute of the NC substream of BIOMASS stream is changed to 1 which will be calculated later by the calculator block.

The mixture than enters the "DRY FLASH" block which was modelled using FLASH 2-unit operation block. It separates the dried biomass from exhaust.

Dried biomass than enters the DECOMP block which simulates the pyrolysis process. RYIELD unit operation model is used to simulate decomposition of nonconventional biomass into conventional components (C, H, O, N, S) [55]. Initial component yields were entered which were later set by a Fortran block which takes into consideration the ultimate analysis of the biomass feedstock [56].

Decomposed yield than enters the SEPARATO block, which separates the char and hydrogen from other volatiles. Char and hydrogen stream goes to OXIDATIO block modelled by RGibbs unit operation model.

Restrict chemical equilibrium approach was selected and oxidation reactions were specified in the block. Required oxygen was also provided by introducing an air stream. Its flowrate was set using a calculator block. Products of the oxidation block are mixed with the VOLATILES stream from SEP2 block in MIXER and then entered in the REDUCTIO block. Reduction block is used to model the reduction zone of the gasifier, using the RGIBBS reactor which calculates equilibrium using the gibbs free energy minimization method. Reduction reactions were specified in this block with temperature approach option selected [57]. Product stream from REDUCTIO block called syngas than undergoes the syngas clean up unit.

Syngas enters the CYCLONE block modelled by SSplit unit operation, whose function is to separate the solids from the syngas. Stream is then cooled to ambient

temperature using the unit operation model HEAT called COOLER in the flowsheet. Energy released during cooling is recovered using the heat stream Q2. Acid gases such as H_2S is then removed from the stream by passing the syngas through the HESREMOV block.

3.1.2 Inlet Streams Specification

Inlet stream's temperature, pressure, composition, and flowrates are given in the table below;

Table 4. Stream Specifications

Streams	Composition	Temperature	Pressure	Mass Flowrate
BIOMASS	Specified at its Ultimate, Proximate and Sulfonate Analysis	25 ^oC	1 atm	100 kg/hr
AIR0	21% O_2, 79% N_2	100 ^oC	1.01325 bar	800 kg/hr
AIR2	21% O_2, 79% N_2	450 ^oC	1.01325 bar	5 kg/hr (Set using Calculator Block)

3.1.3 Block Specifications

Details of different blocks used to model different stages of the process is given in the table below;

Table 5. Block Specifications

Block	Aspen Name	Purpose	Operating Parameters	
DRIER	RStoic	Reduces the moisture content of the biomass feedstock	0 Gcal/hr	1.01325 bar
DRYFLASH	Flash2	Separates the moisture stream from dry biomass	0 Gcal/hr	1.01325 bar
DECOMP	RYield	Decompose the biomass into its component streams based on ultimate and proximate analysis	500 °C	1.01325 bar
SEPARATO	Sep2	Separates the volatiles from char		
OXIDATIO	RGIBBS	Oxidation of Carbon occurs in this block	950 °C	1.01325 bar
MIXER	Mixer	Oxidation products are mixed with the separated volatiles		0 bar
REDUCTIO	RGibbs	Reduction of mixed stream occurs which produces syngas	789 °C	1.01325 bar
CYCLONE	SSplit	Separates unreacted carbon from syngas		
COOLER	Heater	Reduces the temperature of syngas to send into H_2S Removal unit	300 °C	1.01325 bar
H_2SREMOV	Sep	Separates out H_2S from syngas		

3.1.4 Calculator Blocks

3.1.4.1 Water block

This calculator block sets the final moisture content in dried biomass stream and the fractional conversion of biomass to water.

Following equations were entered in the calculator block;

$$DRIERIN \times \frac{INH2O}{100} = DRIEROUT \times \frac{DRYH2O}{100} + DRIERIN \times CONV \quad \text{(Eq. 1)}$$

$$DRIERIN = DRIEROUT - DRIERIN \times CONV \quad \text{(Eq. 2)}$$

Where,

DRIERIN =Mass flow rate of BIOMASS in stream MBIOAIR

DRIEROUT=Mass flow rate of BIOMASS in stream MBIO H_2O

IN H_2O =Percent moisture in the BIOMASS in stream MBIOAIR

DRY H_2O =Percent moisture in the BIOMASS in stream MBIO H_2O

CONV =Fractional conversion of BIOMASS to H_2O in the block DRIER

Equation 16 is the material balance for water, and equation 17 is the overall material balance. These equations can be combined to yield equation 18:

$$CONV = \frac{INH2O - DRYH2O}{100 - DRYH2O} \quad \text{(Eq. 3)}$$

Use equation 3 in a Calculator block to ensure these three specifications are consistent.

Fortran coding:

F DRY H_2O = 8.910

F CONV = (IN H_2O - DRY H_2O) / (100 - DRY H_2O)

The Calculator block specifies the moisture content of the dried coal and calculates the corresponding conversion of coal to water.

Variable	Information flow	Definition
H2OIN		Compattr-Var Stream=WETBIOMA Substream=NC Component=BIOMASS Attribute=PROXANAL Element=1
CONV		Block-Var Block=DRIER Variable=CONV Sentence=CONV ID1=1
H2ODRY		Block-Var Block=DRIER Variable=COMPATT Sentence=COMP-ATTR ID1=NC ID2=BIOMASS ID3=PROXANAL Element=1

Figure 5. WATER Block Variables

This calculator block is executed before the DRIER block.

3.1.4.2 Combust block

This calculator block sets the yield of different elements in the pyrolysis product stream based on its ultimate analysis.

Dried Biomass → Volatiles (H_2, CO, CO_2, H_2O, CH_4 Equivalent and Tar) + Char (16)

Following variables were defined;

Variable	Information flow	Definition
ULT		Compattr-Vec Stream=DRYBIOMA Substream=NC Component=BIOMASS Attribute=ULTANAL
WATER		Compattr-Var Stream=DRYBIOMA Substream=NC Component=BIOMASS Attribute=PROXANAL Element=1
H2O		Block-Var Block=DECOMP Variable=MASS-YIELD Sentence=MASS-YIELD ID1=H2O ID2=MIXED
ASH		Block-Var Block=DECOMP Variable=MASS-YIELD Sentence=MASS-YIELD ID1=ASH ID2=NC
CARB		Block-Var Block=DECOMP Variable=MASS-YIELD Sentence=MASS-YIELD ID1=C ID2=CISOLID
H2		Block-Var Block=DECOMP Variable=MASS-YIELD Sentence=MASS-YIELD ID1=H2 ID2=MIXED
N2		Block-Var Block=DECOMP Variable=MASS-YIELD Sentence=MASS-YIELD ID1=N2 ID2=MIXED
CL2		Block-Var Block=DECOMP Variable=MASS-YIELD Sentence=MASS-YIELD ID1=CL2 ID2=MIXED
SULF		Block-Var Block=DECOMP Variable=MASS-YIELD Sentence=MASS-YIELD ID1=S ID2=MIXED
O2		Block-Var Block=DECOMP Variable=MASS-YIELD Sentence=MASS-YIELD ID1=O2 ID2=MIXED

Figure 6. COMBUST Block Variables

Fortran coding:

F FACT = (100 - WATER) / 100

F H_2O = WATER / 100

F ASH = UTL(1) / 100 * FACT

F CARB = UTL(2) / 100 * FACT

F H_2 = UTL(3) / 100 * FACT

F N_2 = UTL(4) / 100 * FACT

F SULT = UTL(6) / 100 * FACT

F O_2 = UTL(7) / 100 * FACT

Where,

UTL = Vectors, ultimate analysis of BIOMASS

WATER = Percent moisture in the BIOMASS

FACT = Content of BIOMASS in the DBIOMASS

H_2O = Content of H_2O in the pyrolysis products

CARB = Content of CO_2 in the pyrolysis products

H_2 = Content of H_2 in the pyrolysis products

N_2 = Content of N_2 in the pyrolysis products

SULT = Content of S in the pyrolysis products

O_2 = Content of O_2 in the pyrolysis products

ASH = Content of ash in the pyrolysis products

COMBUST calculator block was operated before the DECOMP block.

3.1.4.3 B2 block

Calculates the flowrate of air into the oxidation block depending on the specific Air to Fuel ratio required to ensure proper oxidation and reduction process.

Variable	Information flow	Definition
BIOMASS	Import variable	Stream-Var Stream=DRYBIOMA Substream=NC Variable=MASS-FLOW Units=kg/hr
AIR	Export variable	Stream-Var Stream=AIR2 Substream=MIXED Variable=MASS-FLOW Units=kg/hr

Figure 7. B2 Block Variables

Equation entered in the fortran block was;

F AIR= 1.53*BIOMASS

3.1.5 Efficiency Calculations

In order to access the performance of the modelled gasifier, various parameters were identified to analyse the efficiency of the gasifier. With the known composition of produced syngas, it is also possible to estimate the calorific heating value of the product gas, carbon conversion during the gasification process and cold gas efficiency.

3.1.5.1 Low Heating Value of the produced syngas

LHV of the syngas depends on the percentage of H_2, CO, and CH_4 in the product stream. It can be calculated using the below given formula;

LHV (product gas) = X H_2LHV H_2 +XCOLHVCO + X CH_4LHV CH_4 (Eq. 4)

Standard heating values of the product gas are given in the table below;

Table 6. Standard Heating Values of H_2, CO, CO_2, and CH_4

Gases	**H_2**	**CO**	**CO_2**	**CH_4**
HHV (MJ/Nm^3)	12.74	12.63	0	39.82
LHV (MJ/Nm^3)	10.78	12.63	0	35.88

3.1.5.2 Cold Gas Efficiency

Cold gas efficiency is also a parameter to analyse the performance of gasifier. It calculates the energy which is transferred from biomass to product syngas.

It can be calculated using the following equation;

$$CGE = (mf(gas) * LHVgas)/(mf(biomass) * LHVbiomass) \quad \text{(Eq. 5)}$$

It is called cold gas efficiency as it does not consider the product gas to be at very high temperature.

Higher the CGE, higher the carbon conversion.

3.1.5.3 Carbon Conversion

Carbon conversion is another parameter used to analyse the efficiency of the gasification process. It is the ratio between the mass fraction of carbon in the product stream to carbon in the biomass.

It is given by the formula;

$$C_{conversion} = \frac{m_{f,CO_{(db)}} + m_{f,CO_{2}(db)} + m_{f,CH_{4}(db)}}{m_{f,C,biomass_{(db)}}} \times 100\% \quad \text{(Eq. 6)}$$

3.1.5.4 H_2/CO Ratio:

H_2/CO ratio is defined as;

$$H_2/CO = Vol\ \%\ of\ H_2(dry\ basis)/\ Vol\%\ of\ CO\ (dry\ basis) \quad \text{(Eq. 7)}$$

3.2 SOFC Modeling

In this section, SOFC is modelled using Aspen Plus Simulator. Tubular SOFC technology is modelled. In tubular SOFC, single cells are stacked together to step up the voltage and power output. Electrochemical reactions in a tubular stack depend upon stack and cell geometry, operating temperature and pressure, syngas composition, and current density[58]. There is no Aspen Plus block model which can represent SOFC. Equilibrium reactors utilizing RGibbs free energy minimization method was used to model the main SOFC, however, other unit operation models with minimum requirements of linking to a subroutine were used to model the whole SOFC system. Tubular SOFC technology developed by Siemes-Westinghouse Model with internal reforming, is modelled in this study [59]–[61]. Model performs mass and energy balance and voltage calculations. Voltage calculations were implemented using Fortran block options in sensitivity analysis block of model analysis tools.

Peng Robinson equation of state with the Boston-Mathias alpha function (PR-BM), was specified as the property method to calculate thermodynamic properties of the components. PR-BM is used for processes involving, nonpolar and mildly polar mixtures such as light gases and hydrocarbons. Units were set to METCBAR, which uses metric system units. All the components in the process were than specified as conventional components. In the simulation mode, stream class was set to CONVEN. It is used when no solids are present, and only mixed stream is present.

3.2.1 Flowsheet Development

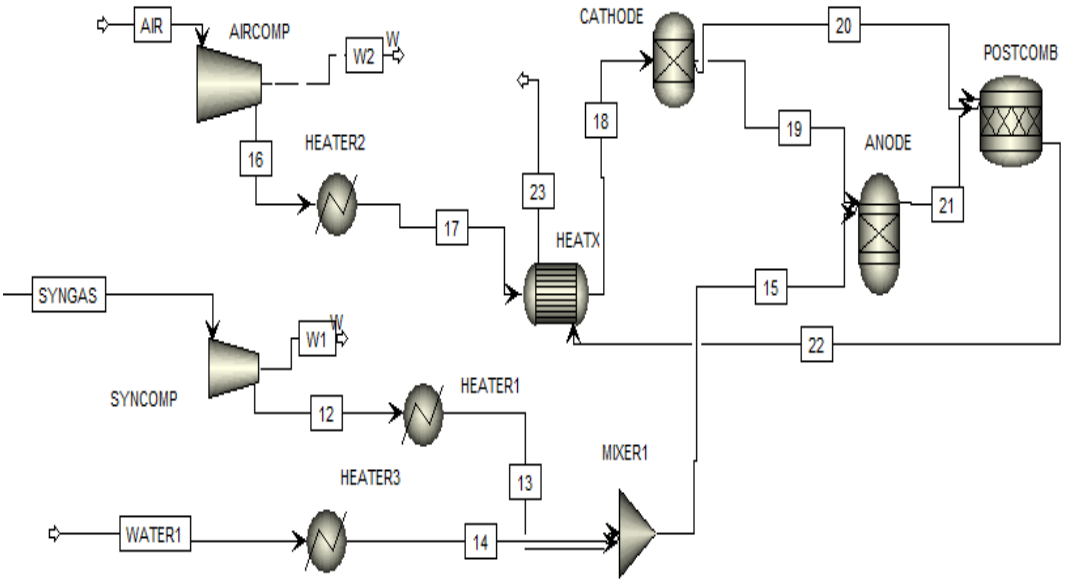

Figure 8. Aspen Plus SOFC Flowsheet

Main Assumptions:

- The whole process is isothermal and steady-state
- 0-D model
- Reforming and shift reactions reach chemical equilibrium
- Overall oxidation of H_2 is considered since movement of ions through electrolyte cannot be modelled
- CO is shifted to H_2 and CH_4 is reformed to H_2 [62]–[65]
- Blocks are considered zero-dimensional, characterized by uniform temperature and perfect mixing
- Residence time is enough to reach equilibrium in the R-Gibbs block
- The system operates in a steady state condition and the changes in kinetic and potential energies are negligible.
- Heat loss from the components and the connecting pipes is negligible.
- Contact resistances are negligible.
- Unreacted gases are assumed to be fully oxidized in the afterburner

Syngas first enters the compressor which increases its pressure slightly to make it flow through the model. Compressor is operated at 90% efficiency. Syngas operating conditions were entered. Its initial flowrate was set to 1kmol/hr which will be later defined by the required output power of the SOFC. Syngas was then heated to the

preheating temperature in HEATER1 and then send to anode which is modelled using RGibbs Equilibrium reactor using the restrict chemical equilibrium approach. Internal reforming equations and overall reaction equation are entered in this block.

Internal Reforming reactions are given by equation 17 and 18;

Steam Reforming: $CH_4 + H_2O \rightarrow 3H_2 + CO$ (17)

CO-Shift Reaction: $CO + H_2O \rightarrow CO_2 + H_2$ (18)

Overall Reaction is the combination of reactions occurring at anode and cathode given by equation 19;

Overall Reaction: $H_2 + 0.5\ O_2 \rightarrow H_2O$ (19)

In anode, CH_4 is reformed to H_2, CO is shifted to CO_2, and H_2 is oxidized. These reactions reach equilibrium at the operating temperature of anode. Hydrogen consumed in the overall reaction is the one produced in equation 17 and 18 as well as any hydrogen coming in with the syngas stream. Air at operating conditions is then introduced in another stream. Its initial flowrate is first set to 50 kmol/hr which will be later defined using a design specification block which varies the air flowrate till air utilization factor becomes equal to a specified value. Air utilization factor (Ua) is the ratio of oxygen utilized in SOFC to oxygen entered in SOFC.

$$Ua = (n\ O_2 Consumed)/(n\ O_2 IN) \quad \text{(Eq. 8)}$$

Where n O_2Consumed is calculated using the following set of equations;

$$n\ O_2 Consumed = 0.5 n\ H_2 Consumed \quad \text{(Eq. 9)}$$

$$n\ H_2 Consumed = Uf\ x\ N\ H_2 IN \quad \text{(Eq. 10)}$$

$$n\ H_2 IN = n\ H_2\ syngas + 1(n\ COsyngas) + 4(n\ CH_4 syngas) \quad \text{(Eq. 11)}$$

n H_2syngas is molar flowrate of H_2 in syngas, nCOsyngas is molar flowrate of CO in SYNGAS stream, and CH_4syngas is molar flowrate of CH_4 in syngas stream. Uf is the fuel utilization factor which represents the conversion of fuel into water.

The AIR stream then enters a compressor AIRCOMP block, which compresses the air slightly to make it flow through the SOFC. Compressor isentropic efficiency is

set to 85%. Compressed air than pass through a heat exchanger HEATX2. In HEATX2 AIR stream gets heated by the combustion products stream. Air stream is further reheated to SOFC's operating temperature using HEATER2. In SOFC, air stream further gets heated by the electrochemical reactions, here HEATX2 and HEATER2 simulate that. Air stream than enters the CATHODE block, which separates the O_2 required by the electrochemical reactions. Separated O_2 than enters the anode. This step models the oxygen ion cross over to the anode.

In anode, SYNGAS and O_2 undergoes electrochemical reactions. Anode-off gas than enters the POSTCOMBUSTION chamber which is modelled using the RSTOIC reactor which is used when we know the fractional conversion or the extent of reaction. Complete combustion is assumed.

Combustion reactions are;

Hydrogen oxidation: $H_2 + O_2 = H_2O$ (20)

Carbon monoxide oxidation: $CO + O_2 = CO_2$ (21)

3.2.2 Inlet Streams Specification

Inlet stream's temperature, pressure, composition, and flowrates are given in the table below;

Table 7. Stream Specifications for SOFC

Streams	Composition	Temperature	Pressure	Mass Flowrate
SYNGAS	Specified at its Ultimate, Proximate and Sulfonate Analysis	300 ^{o}C	1.01325 bar	Set using Design Specification block depending upon power output
AIR	21% O_2, 79% N_2	25 ^{o}C	1.01325 bar	5 kmol/hr (Set using Design Spec Block depending upon UA)
WATER1	100% H_2O	25 ^{o}C	1.01325 bar	0.5 kmol/hr (Set using Design Spec Block depending upon STCR)

3.2.3 Block Specifications

Detail of blocks used in simulating SOFC is given in table below;

Table 8. Block Specifications for SOFC

Block	Aspen Name	Purpose	Operating Parameters	
SYNCOMP	Compr	Increases the pressure of incoming syngas to make it flow through the system		1.097 bar
HEATER1	Heater	Increases the temperature of the pressurized syngas	900 ^{o}C	Delta P =0
AIRCOMP	Compr	Compresses the air slightly to make it flow through the system	500 ^{o}C	1.097 bar
HEATER2	Heater	Increases the temperature of air to specified air temperature from literature	630 ^{o}C	Delta P = 0
HEATX	HeatX	Further increases the temperature of air to undergo reactions at anode	Cold Stream outlet T = 800 ^{o}C (Later set using DS Block)	Delta P =0
HEATER3	Heater	Increases the temperature of incoming water stream	T = 610 ^{o}C	Delta P =0
MIXER1	Mixer	Mixes syngas with water to reach specified STCR		
ANODE	RGibbs	Reforming as well as electrochemical reactions take place	T = 910 ^{o}C	Delta P =0
CATHODE	Sep	Separates the O_2 required at anode depending upon UA		
POSTCOMB	RStoic	Complete combustion of the anode off gas takes place	T = 900 ^{o}C	Delta P =0

3.2.4 Design Specification blocks

3.2.4.1 AIR block

This block is used to set the flowrate of air into SOFC, depending upon the air utilization factor.

Variables defined are;

Variable	Definition
H2	Mole-Flow Stream=SYNGAS Substream=MIXED Component=H2 Units=kmol/hr
CO	Mole-Flow Stream=SYNGAS Substream=MIXED Component=CO Units=kmol/hr
CH4	Mole-Flow Stream=SYNGAS Substream=MIXED Component=CH4 Units=kmol/hr
FAIR	Stream-Var Stream=19 Substream=MIXED Variable=MOLE-FLOW Units=kmol/hr
XO2	Mole-Frac Stream=19 Substream=MIXED Component=O2

Figure 9. AIR Block Variables

SPEC : FAIR*X O_2*0.167

TARGET : 0.85*(H_2 + CO + 4.0* CH_4)*0.5

TOLERANCE : 0.1

3.2.4.2 SYNWATER block

This design specification block sets the flowrate of water which is mixed with syngas, depending upon the specified steam to carbon ratio.

Steam to Carbon Ratio is given by;

STCR = Moles of Carbon/Moles of H_2O

STCR = (NCO+N CO_2+N CH_4)/N H_2O

Variables defined were;

Variable	Definition
H2O	Mole-Flow Stream=SYNGAS Substream=MIXED Component=H2O Units=kmol/hr
CH4	Mole-Flow Stream=SYNGAS Substream=MIXED Component=CH4 Units=kmol/hr
CO	Mole-Flow Stream=SYNGAS Substream=MIXED Component=CO Units=kmol/hr
CO2	Mole-Flow Stream=SYNGAS Substream=MIXED Component=CO2 Units=kmol/hr
H2OIN	Stream-Var Stream=WATER1 Substream=MIXED Variable=MOLE-FLOW Units=kmol/hr

Figure 10. SYNWATER Block Variables

SPEC : $H_2OIN + H_2O$

TARGET : $2.5*(CH_4+CO+ CO_2)$

TOLERANCE : 0.1

3.2.5 Calculator Blocks

3.2.5.1 TANODE block

This block is used to set the temperature of HEATER1 block which heats the incoming syngas to preheating temperature. Its temperature is set around 300 ^{O}C less than the SOFC's operating temperature.

Variables defined are;

Variable	Information flow	Definition
ANODEGAS	Export variable	Block-Var Block=HEATER1 Variable=TEMP Sentence=PARAM Units=C
SOFC	Import variable	Block-Var Block=ANODE Variable=TEMP Sentence=PARAM Units=C

Figure 11. TANODE Block variables

Fortran Coding:

F ANODEGAS = SOFC-300

3.2.5.2 TCATHODE Block

This calculator block calculates the temperature of the air stream when leaving the heat exchanger. It is set around 100 degrees less than SOFC.

Variables defined are;

Variable	Information flow	Definition
CATHOGAS	Export variable	Block-Var Block=HEATX Variable=T-COLD Sentence=PARAM Units=C
SOFC	Import variable	Block-Var Block=ANODE Variable=TEMP Sentence=PARAM Units=C

Figure 12. TCATHODE Block Variables

Fortran Coding:

F CATHOGAS = SOFC-100

3.2.5.3 TWATER block

Sets the temperature of block HEATER3, which preheats the incoming water stream.

Variables defined are;

Variable	Information flow	Definition
WHEAT	Export variable	Block-Var Block=HEATER3 Variable=TEMP Sentence=PARAM Units=C
SYNTEMP	Import variable	Stream-Var Stream=13 Substream=MIXED Variable=TEMP Units=C

Figure 13. TWATER Block Variables

Fortran Coding:

F WHEAT = SYNTEMP

3.2.6 Voltage Calculations

Voltage of the SOFC is calculated by first calculating the Nernst Voltage (ideal voltage), and then subtracting various voltage losses from the ideal voltage.

$$\mathbf{V_N} = \frac{-\Delta g_f}{2.F} + \frac{R_g.T_{avg}}{2.F} \ln \frac{P_{H_2}.P_{O_2}^{0.5}}{P_{H2O}} \qquad \text{(Eq. 12)}$$

Where,

Δg_f = molar Gibbs free energy of formation (J/mol) at standard pressure (1 bar), and 2 represents the number of moles of electrons produced per mole of H_2 fuel reacted,

F = Faraday constant (96,485 C/mol),

T_{avg} = average temperature between the SOFC inlet and outlet streams (K),

R_g = universal gas constant (8.314J/mol.K) and

P_i= partial pressure (in bar) of gaseous component i.

Voltage Losses can be divided into three main categories;

1. Ohmic Loss
2. Activation Loss
3. Concentration Loss

Details of these losses is given below;

3.2.6.1 Ohmic Loss

Loss in voltage which results because of the resistance which electrons face during their movement through electrodes and interconnections, and the resistance which ions face while their flow through electrolyte. Ohmic loss is the highest in tubular SOFC's because of the long current flow paths through it.

Following equations (33-36) are used to calculate ohmic losses through different components [66];

$$V_{Ohm\_A} = \frac{j.\rho_A(A.\pi.D_m)^2}{8.t_A} \quad \text{(Eq. 13)}$$

$$V_{Ohm\_C} = \frac{j.\rho_C(\pi.D_m)^2}{8.t_C} \cdot A[A + 2(1 - A - B)] \quad \text{(Eq. 14)}$$

$$V_{Ohm\_E} = j.\rho_E.t_E \quad \text{(Eq. 15)}$$

$$V_{Ohm\_Int} = j.\rho_{Int}(\pi.D_m)\frac{t_{Int}}{w_{Int}} \quad \text{(Eq. 16)}$$

Where,

$A.\pi$ = angle related to the extent of electrical contact

$B.\pi$ = angle related to the interconnection.

j = current density (A/m^2),

D_m = mean diameter of a cell (m),

t = the cell component thickness (m)

w_{Int} = interconnection width (m)

ρ_A = Anode resistivity (Ωm)

ρ_C = Cathode resistivity (Ωm)

ρ_E = Electrolyte resistivity (Ωm)

ρ_{Int} = Interconnection resistivity (Ωm)

These resistivity terms are determined using the temperature dependent relations given in equations (37-40) [67], [68]

Anode resistivity ρ_A (Ωm)	$2.98 \times 10^{-5} \exp(-1392/T_{op})$	(Eq. 17)
Cathode resistivity ρ_C (Ωm)	$8.114 \times 10^{-5} \exp(600/T_{op})$	(Eq. 18)
Electrolyte resistivity ρ_E (Ωm)	$2.94 \times 10^{-5} \exp(10350/T_{op})$	(Eq. 19)
Interconnection resistivity ρ_{Int} (Ωm)	0.025	(Eq. 20)

3.2.6.2 Activation Loss

It is the loss due to the energy barrier which reacting species need to overcome at electrodes. Because of high operating temperature, activation loss is less in SOFC's.

Activation loss at anode and cathode are given by the following equations;

Anode:

$$\frac{1}{R_{Act\_A}} = \frac{2.F}{R_g.T_{op}} \cdot k_A \left(\frac{P_{H_2}}{P^0}\right)^m exp\left(\frac{-E_A}{R_g.T_{op}}\right) \quad \text{(Eq. 21)}$$

Cathode:

$$\frac{1}{R_{Act\_C}} = \frac{4.F}{R_g.T_{op}} \cdot k_C \left(\frac{P_{O_2}}{P^0}\right)^m exp\left(\frac{-E_C}{R_g.T_{op}}\right) \quad \text{(Eq. 22)}$$

Where,

R_{Act_C} = specific resistance (Ωm^2) at cathode

R_{Act_A} = specific resistance (Ωm^2) at anode

P_i = partial pressures (bar) which were taken as average values of the pressure of anode and cathode inlet and outlet streams (0-D model).

P^0 = reference pressure, taken as 1 bar;

E_A = Activation Energy at Anode

E_C = Activation Energy at Cathode

k_A = pre-exponential factors for Anode

k_C =. pre-exponential factor for Cathode

3.2.6.3 Concentration Loss

Loss because of the mass transfer limitation in porous electrodes.

Concentration losses at anode and cathode can be calculated by following equations (43,44);

$$V_{Conc\_A} = -\frac{R_g.T_{op}}{2.F} \ln\left[\frac{1-(R_g.T_{op}/2.F)\left(t_A/D_{An(eff)}.y^0_{H_2}.P_{SOFC}\right)j}{1+(R_g.T_{op}/2.F)(t_A/D_{An(eff)}.y^0_{H2O}.P_{SOFC})j}\right] \quad \text{(Eq. 23)}$$

$$V_{Conc\_C} = -\frac{R_g.T_{op}}{4.F} \ln\left\{\frac{(P_{SOFC}/\delta_{O_2})-\left[(P_{SOFC}/\delta_{O_2})-y^0_{O_2}.P_{SOFC}\right]exp[(R_g.T_{op}/4.F)(\delta_{O_2}.t_C/D_{Cat(eff)}.P_{SOFC})j]}{y^0_{O_2}.P_{SOFC}}\right\}$$

(Eq. 24)

$y^0_{H_2}$ = average values of gas molar fraction of H_2 in the inlet and outlet streams of anode

y^0_{H2O} = average values of gas molar fraction of H_2O in the inlet and outlet streams of anode

$y^0_{O_2}$ = average values of gas molar fraction of O_2 in the inlet and outlet streams of cathode

$D_{Cat(eff)}$ = diffusion coefficient cathode

$D_{An(eff)}$ = diffusion coefficient anode

For diffusion coefficient calculations; both ordinary and Knudsen diffusion are considered. Ordinary diffusion occurs when pores of electrode are larger than the mean free path of gas molecules, while Knudsen diffusion occurs when pores are smaller than the mean free path.

Equation 45 and 46 are used to calculate ordinary binary diffusion and effective ordinary binary diffusion coefficients;

$$D_{ik} = \frac{1 \times 10^{-7} {T_{op}}^{1.75} (1/M_i + 1/M_k)^{1/2}}{P\left({v_i}^{1/3} + {v_k}^{1/3}\right)^2} \qquad \text{(Eq. 25)}$$

$$D_{ik(eff)} = D_{ik}(\varepsilon/\xi) \qquad \text{(Eq. 26)}$$

Where,

subscripts i and k = the gaseous components that make up the

binary gas mixture (H_2- H_2O at the anode and O_2- N_2 at the cathode),

P = Atmospheric pressure and

v = Fuller diffusion volume,

taken as 7.07, 12.7, 16.6 and 17.9 for H_2, H_2O, O_2 and N_2 respectively

Mi = molecular weight (kg/Kmol) of the gaseous component

ε = porosity of electrodes

ξ = tortuosity of electrodes

Equation 47 and 48 are used to calculate Knudsen diffusion and effective Knudsen diffusion coefficients;

$$D_{K,i} = 97r\left(T_{op}/M_i\right)^{0.5} \quad \text{(Eq. 27)}$$

$$D_{K,i(eff)} = D_{K,i}(\varepsilon/\xi) \quad \text{(Eq. 28)}$$

Overall effective diffusion coefficient for each gas was then calculated using the below equation;

$$1/D_{i(eff)} = 1/D_{ik(eff)} + 1/D_{K,i(eff)} \quad \text{(Eq. 29)}$$

Then anode and cathode diffusion coefficients were calculated using the given equation 50 and 51;

$$D_{An(eff)} = \left(\frac{y^0_{H_2O} \cdot P_{SOFC}}{P_{SOFC}}\right) D_{H_{2(eff)}} + \left(\frac{y^0_{H_2} \cdot P_{SOFC}}{P_{SOFC}}\right) D_{H_2O_{(eff)}} \quad \text{(Eq. 30)}$$

$$D_{Cat(eff)} = D_{O_2(eff)} \quad \text{(Eq. 31)}$$

Constant Sigma δ_{O_2} is calculated using the below equation;

$$\delta_{O_2} = \frac{D_{K,O_2(eff)}}{\left(D_{K,O_2(eff)} + D_{O_2-N_2(eff)}\right)} \quad \text{(Eq. 32)}$$

Where,

I = gaseous components (H_2, H_2O, O_2 or N_2),

r = electrode pore radius (m)

Actual cell Voltage is then calculated by subtracting voltage losses from Nernst voltage.

$$V = VN - V_{ohm} - V_{conc} - V_{act} \quad \text{(Eq. 33)}$$

3.2.6.4 Model Parameters:

Model Parameters for SOFC are given in the below table;

Table 9. Model Parameters for SOFC

Geometry [47], [68]–[70]	
Cell length/diameter (m)	1.5 / 0.022
Anode thickness (m)	0.0001
Cathode thickness (m)	0.0022
Electrolyte thickness (m)	0.00004
Interconnection thickness (m)	0.000085
Interconnection width (m)	0.009
Ohmic Loss [66]	
A/B	0.804 / 0.13
Activation Loss [64], [71]	
Pre-exponential factor K_A / K_C (A/m^2)	2.13×10^8 / 1.49×10^{10}
Slope m	0.25
Activation Energy E_A / E_C (J/mol)	110000 / 160000
Concentration Loss [72], [73]	
Electrode pore radius r (m)	5×10^{-7}
Electrode Porosity / Torosity	0.5 / 5.9

3.2.7 Power and Efficiency Calculations

Current is then calculated using the following equations;

$$Current\ (I) = 2\ x\ F\ x\ (n\ H2IN) \quad \text{(Eq. 34)}$$

$$n\ H2IN = n\ FuelIN\ x\ (y\ H2 + yCO + 4y\ CH4)\ x\ UF \quad \text{(Eq. 35)}$$

Current density is then calculated by dividing current with the area,

$$Current\ Density\ (j) = Current\ (I)/Area\ (A) \quad \text{(Eq. 36)}$$

Gross and Net Efficiency Calculations of SOFC:

$$\eta_{SOFC,gross} = \frac{P_{el,AC}}{nFuel_{in}.LHV_{fuel}} \quad \text{(Eq. 37)}$$

$$\eta_{SOFC,net} = \frac{P_{el,AC} - P_{comp}}{nFuel_{in}.LHV_{fuel}} \quad \text{(Eq. 38)}$$

Where,

$P_{el,AC}$ = AC power (kW),

$nFuel_{in}$ = molar flow rate of input fuel (kmol/s),

LHV_{fuel} = lower heating value of the input fuel (kJ/kmol) and

P_{comp} = electrical power requirement of the fuel and air compressors (kW)

Summary

In this section, modeling of gasifier and SOFC is explained. Flowsheet for both the systems is developed, details of unit operation blocks is also added, together with different operating parameters and conditions. Efficiency calculations for both the systems, and voltage calculation for SOFC is also explained.

References

[53] D. Peng and D. B. Robinson, "A New Two-Constant Equation of State," *Ind. Eng. Chem. Fundam.*, vol. 15, no. 1, pp. 59–64, Feb. 1976.

[54] I. Aspen Technology, "Aspen Plus ® User Guide," *Aspen Technol. Inc.*, p. 936, 2000.

[55] S. M. Atnaw, S. A. Sulaiman, and S. Yusup, "A Simulation Study of Downdraft Gasification of Oil-Palm Fronds using ASPEN PLUS," *J. Appl. Sci.*, vol. 11, no. 11, pp. 1913–1920, Nov. 2011.

[56] R. Sotudeh-Gharebaagh, R. Legros, J. Chaouki, and J. Paris, "Simulation of circulating fluidized bed reactors using ASPEN PLUS," *Fuel*, vol. 77, no. 4, pp. 327–337, Mar. 1998.

[57] W. Doherty, A. Reynolds, and D. Kennedy, "Aspen Plus Simulation of Biomass Gasification in a Steam Blown Dual Fluidised Bed," *Book/b. Chapters*, Aug. 2013.

[58] A. V. Akkaya, B. Sahin, and H. Huseyin Erdem, "Exergetic performance coefficient analysis of a simple fuel cell system," *Int. J. Hydrogen Energy*, vol. 32, no. 17, pp. 4600–4609, Dec. 2007.

[59] S. E. Veyo, "The Westinghouse solid oxide fuel cell program-a status report," in *IECEC 96. Proceedings of the 31st Intersociety Energy Conversion Engineering Conference*, vol. 2, pp. 1138–1143.

[60] S. E. Veyo and W. L. Lundberg, "Solid Oxide Fuel Cell Power System Cycles," in *Volume 2: Coal, Biomass and Alternative Fuels; Combustion and Fuels; Oil and Gas Applications; Cycle Innovations*, 1999, p. V002T02A058.

[61] S. C. Singhal, "Recent Progress in Tubular Solid Oxide Fuel Cell Technology," *ECS Proc. Vol.*, vol. 1997–40, pp. 37–50, Jan. 1997.

[62] P. Costamagna, L. Magistri, and A. F. Massardo, "Design and part-load performance of a hybrid system based on a solid oxide fuel cell reactor and a micro gas turbine," *J. Power Sources*, vol. 96, no. 2, pp. 352–368, Jun. 2001.

[63] W. Zhang, E. Croiset, P. L. Douglas, M. W. Fowler, and E. Entchev, "Simulation of a tubular solid oxide fuel cell stack using AspenPlusTM unit operation models," *Energy Convers. Manag.*, vol. 46, no. 2, pp. 181–196, Jan. 2005.

[64] P. Hofmann, K. D. Panopoulos, L. E. Fryda, and E. Kakaras, "Comparison between two methane reforming models applied to a quasi-two-dimensional

planar solid oxide fuel cell model," *Energy*, vol. 34, no. 12, pp. 2151–2157, Dec. 2009.

[65] K. D. Panopoulos, L. E. Fryda, J. Karl, S. Poulou, and E. Kakaras, "High temperature solid oxide fuel cell integrated with novel allothermal biomass gasification: Part I: Modeling and feasibility study," *J. Power Sources*, vol. 159, no. 1, pp. 570–585, Sep. 2006.

[66] T. W. Song, J. L. Sohn, J. H. Kim, T. S. Kim, S. T. Ro, and K. Suzuki, "Performance analysis of a tubular solid oxide fuel cell/micro gas turbine hybrid power system based on a quasi-two dimensional model," *J. Power Sources*, vol. 142, no. 1–2, pp. 30–42, Mar. 2005.

[67] N. F. Bessette, W. J. Wepfer, and J. Winnick, "A Mathematical Model of a Solid Oxide Fuel Cell," *J. Electrochem. Soc.*, vol. 142, no. 11, p. 3792, Nov. 1995.

[68] S. Campanari and P. Iora, "Definition and sensitivity analysis of a finite volume SOFC model for a tubular cell geometry," *J. Power Sources*, vol. 132, no. 1–2, pp. 113–126, May 2004.

[69] M. . Williams, J. . Strakey, and S. C. Singhal, "U.S. distributed generation fuel cell program," *J. Power Sources*, vol. 131, no. 1–2, pp. 79–85, May 2004.

[70] F. Calise, M. Dentice d' Accadia, L. Vanoli, and M. R. von Spakovsky, "Full load synthesis/design optimization of a hybrid SOFC–GT power plant," *Energy*, vol. 32, no. 4, pp. 446–458, Apr. 2007.

[71] E. Achenbach, "Three-dimensional and time-dependent simulation of a planar solid oxide fuel cell stack," *J. Power Sources*, vol. 49, no. 1–3, pp. 333–348, Apr. 1994.

[72] S. . Chan, K. . Khor, and Z. . Xia, "A complete polarization model of a solid oxide fuel cell and its sensitivity to the change of cell component thickness," *J. Power Sources*, vol. 93, no. 1–2, pp. 130–140, Feb. 2001.

[73] F. Calise, A. Palombo, and L. Vanoli, "One-Dimensional Model of a Tubular Solid Oxide Fuel Cell A Smart renewable energy system for Campania Region (IT)-Strategies and actions towards the achievements of the 2030 European targets. View project The 1st Latin American Conference on Sustainable Development of Energy, Water and Environment Systems-1st LA SDEWES Rio de Janeiro View project Massimo Dentice d'Accadia One-Dimensional Model of a Tubular Solid Oxide Fuel Cell," *Artic. J. Fuel Cell Sci. Technol.*, 2008.

Chapter 4: Results and Discussion

4.1 Biomass Gasification

4.1.1 Model Validation

The simulated biomass gasification model was validated using the experimental data from [74]Wei et al, in which hardwood chips were gasified in pilot-scale downdraft gasifier unit using air as gasifying agent.

Experimental Run # 14 was selected to validate the model. Operating parameters for this experimental run are given in the below table.

Table 10. Gasifier Operating Parameters

Biomass Feeding Rate	20.58 kg/hr
Operating Temperature	850 ^{O}C
Moisture Content	10 %
Equivalence Ratio	0.2544

Equivalence ratio is calculated by relation proposed by Gagliano et al. [75], [76] , according to it;

$$\text{Equivalence Ratio (ER)} = 0.008 \text{ X M.C} + 0.174$$

This correlation is used to limit the underestimation of CH_4 in thermodynamic equilibrium models of gasification.

Model was run on the above mentioned operating conditions. The ultimate and proximate analysis used in this study given in table 3333 was also used for the modeling [77], [78].

Table 11. Ultimate and Proximate analysis of Hardwood chips

Ultimate Analysis (Dry Basis)		
Carbon	wt. %	49.817
Hydrogen	wt. %	5.556
Oxygen	wt. %	43.425
Nitrogen	wt. %	0.078
Sulphur	wt. %	0.005
Ash	wt. %	1.119
Total	wt. %	100
Proximate Analysis (Dry basis)		
Volatile Matter	wt. %	79.85
Fixed Carbon	wt. %	19.031
Ash	wt. %	1.119
Total	wt. %	100
Moisture (received basis)	wt. %	25
Moisture (After pre-drying)	wt. %	8.91
HHV (dry basis)	MJ/Kg	18.58
Bulk Density	kg/m3	222.15

The model results were in good agreement with the experimental results for that run. Statistical Analysis was done to analyse the accuracy of results. RSS, MRSS, and Mean Error were calculated for this purpose[79].

Table 12. Model Validation

Components	**Literature**	**Our Model**
H_2	0.1912	0.2185
CO	0.2376	0.261301
CH_4	0.0310	0.000368957
CO_2	0.1096	0.0789949
LHV (MJ/Nm3)	6.17	5.669

4.1.2 Sensitivity Analysis

Parameters Affecting the Gasifier's Performance;

1. Moisture Content
2. Gasification Temperature
3. Equivalence Ratio
4. Gasifying Agent

4.1.2.1 Gasifying Agent

Other than the type of gasifier and category of feedstock, operating conditions and gasifying agent also affects the producer gas. Air, being readily available and economical is one of the most common gasifying agent. It produces a nitrogen diluted (around 50 vol%) gas having low heating value (around 4-6 MJ/Nm3 HHV) [80]. Oxygen alone is also used but is uneconomical. CO_2 alone[81], or in combination with air or O_2 can also be used for gasification [82].

4.1.2.2 Gasification Temperature

Gasification is more efficient at high temperature, however, materials used in the gasifier making limits the gasification temperature to around 1000 ^{O}C [83]. Lower temperatures result in high amounts of char and tar while high temperatures result in high H_2 and CO content.

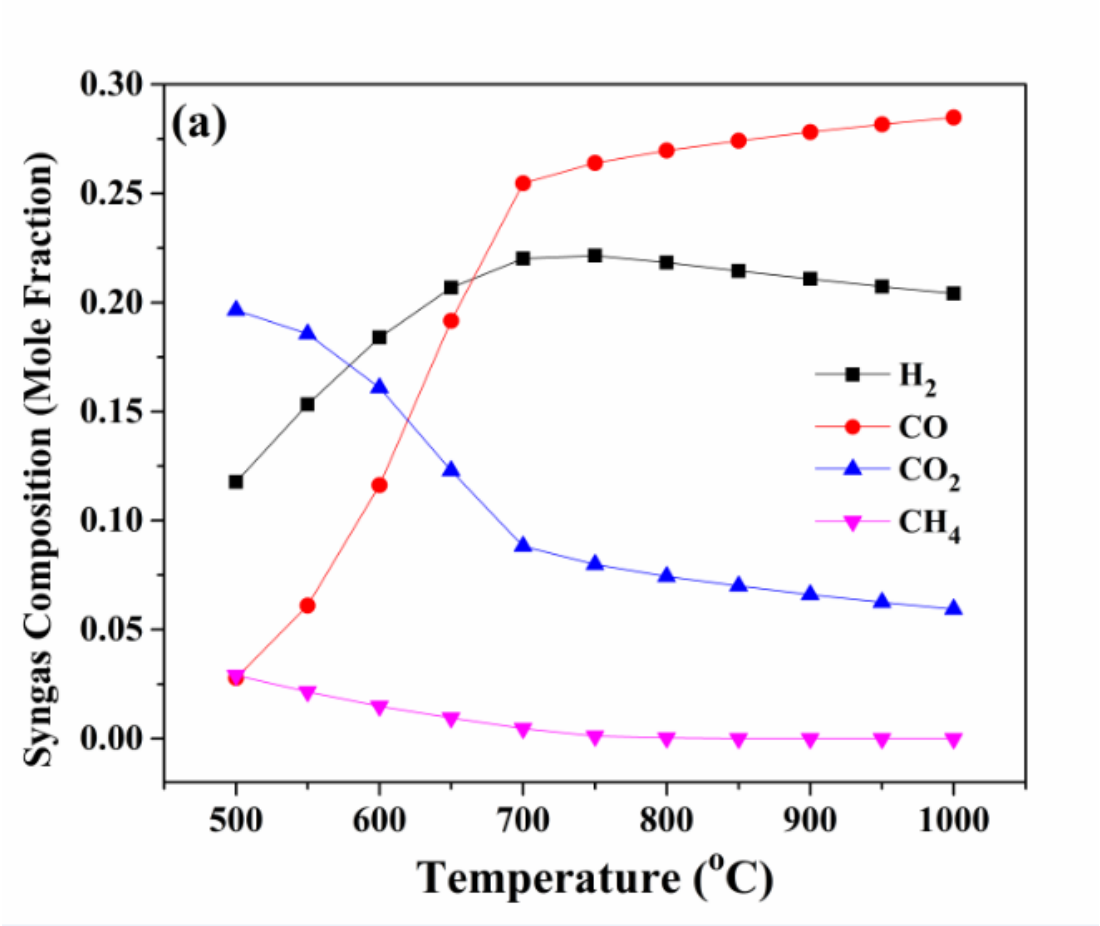

Figure 14. Temperature Vs Composition

The increase in CO and H_2 concentration from 500 to 700 ^oC was because of the combined effect of boudouard, steam methane reforming and water-gas reaction. These reactions are endothermic in nature and thus are favored with increasing temperature. The decrease in CO_2 and CH_4 concentration with increasing temperature was because of the exothermic nature of water gas shift and methanation reaction, making them unfavorable at higher temperatures. The decrease in H_2 concentration after 700 ^oC can be attributed to the combined effect of all the reactions occurring in the reduction zone. At low temperatures, water gas shift reaction contributed to hydrogen production, but this reaction was hindered at high temperatures.

At high temperatures, water gas and steam methane reforming reactions contributed majorly to H_2 production, but steam methane reforming reaction was limited by the absence of reactants such as CH_4 at a higher temperature. From these observations, it can be concluded that water gas shift reaction majorly controls the H_2 production. The decrease in CO_2 concentration with the increase in temperature can

be caused by the boudouard reaction which utilizes CO_2 to produce CO and being endothermic in nature is favored at high temperatures. CH_4 produced in methanation reaction was favored at low temperature because of its exothermic nature. Thus, the decrease in CH_4 concentration with an increase in temperature. Cold gas efficiency and LHV first increased abruptly from 26 % at 500 ^oC to 57 % at 700 ^oC and then almost became constant. H_2/CO ratio decreased sharply from 4.5 at 500 ^oC to 0.7 at 700 ^oC and then decreased slightly till 1000 ^oC. The decrease in H_2/CO ratio was because of an abrupt increase in CO concentration till 700 ^oC.

After 700 ^oC, the increase in CO was very less, due to which the decrease in H_2/CO ratio was also very small. LHV increased till 700 ^oC because of increase in H_2, CO, and CH_4 concentrations. After 700 ^oC, LHV did not vary much because of decreasing H_2 concentration and slightly increasing CO concentration. CGE also followed the LHV trend as it is the main factor affecting the cold gas efficiency of the gasifier.

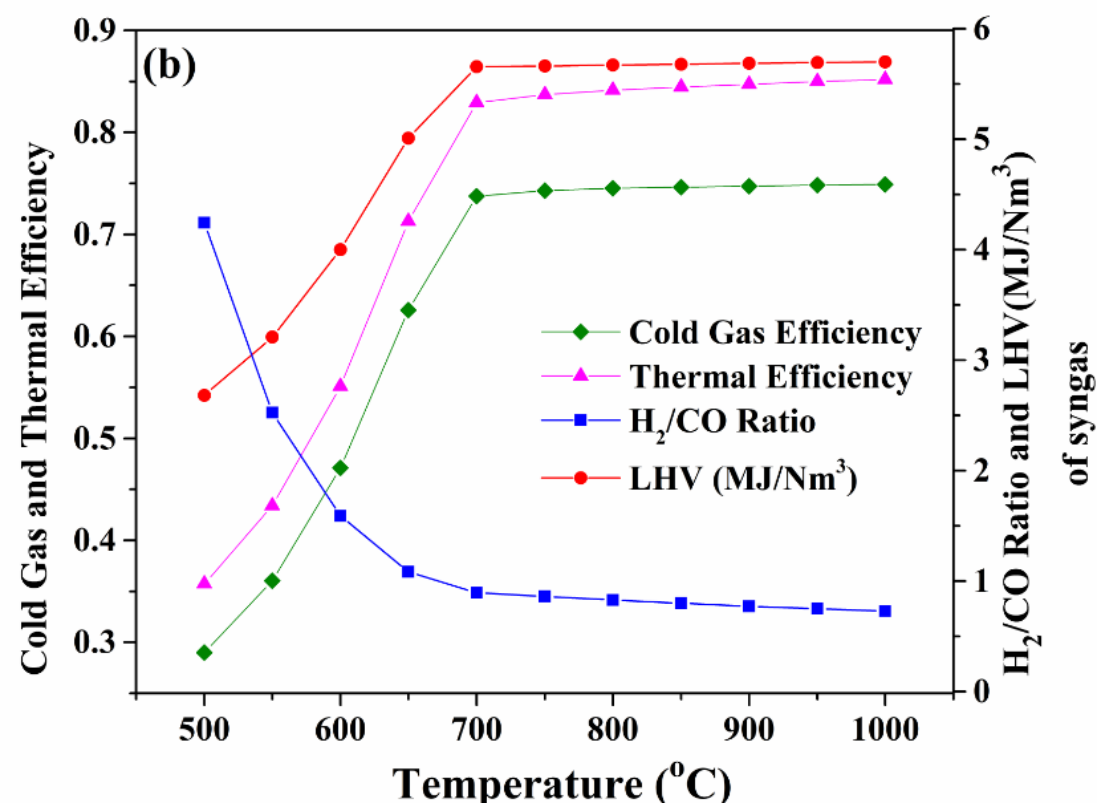

Figure 15. Temperature Vs LHV, CGE, H_2/CO Ratio

4.1.2.3 Equivalence Ratio (ER)

The equivalence ratio (ER) is also a key parameter in gasification process. It is given by; actual air/biomass ratio divided by the stoichiometric air/biomass ratio as with stoichiometric oxidation or complete combustion taking place at ER = 1[28] High equivalence ratios result in low H_2 and co content which in turn results in low heating value of producer gas. ER of 0.2 to 0.4 is considered appropriate to produce syngas with good heating value [84], [85]

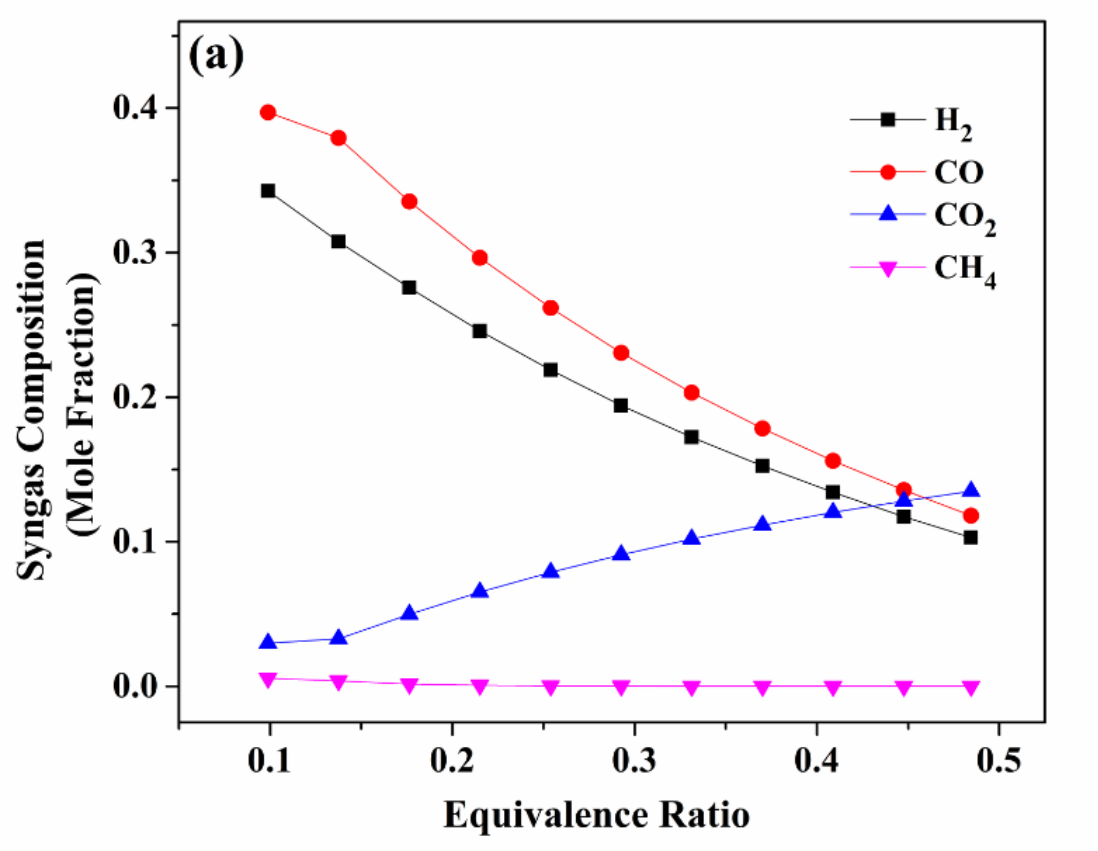

Figure 16. Equivalence Ratio Vs Composition

H_2 and CO concentration decreases with increase in ER, while CO_2 and CH_4 concentration increases with increase in ER. Increase in oxygen supply, increases the ER, which enhances the char combustion and hydrogen combustion reaction, which utilizes C, and H_2 to produce CO_2 and H_2O. H_2 concentration decreases from 0.4 at 0.05 ER to 0.05 at 0.5 ER. CO also followed almost the same trend. CO_2 increased from 0.02 at 0.05 ER to 0.15 at ER =0.5. However, CH_4 almost remained constant.

H_2/CO ratio decreased sharply from 0.05 to 1 ER because the CO concentration was more as compared to H_2 in the beginning and then the difference between the two concentrations decreases with the increase in equivalence ratio. LHV of syngas decreases from 9.5 at ER = 0.05 to 2.5 at ER = 0.5. The decrease in LHV value is because of the decrease in H_2, CO, and CH_4 concentration. Because of the decrease in LHV Cold gas efficiency also decreases with the increase in ER. Slight increase of CGE in the beginning is because CO_2 concentration remains constant in the beginning, causing the overall H_2, CO, and CH_4 concentration to increase adding to LHV of syngas which interns increases the CGE.

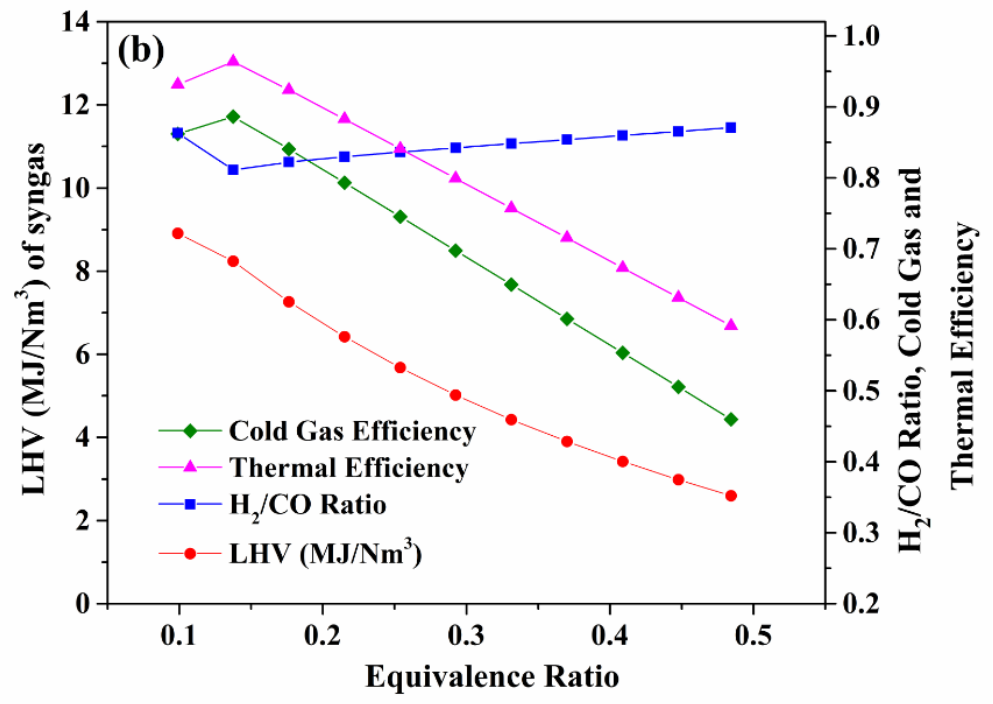

Figure 17. Equivalence Ratio Vs LHV, CGE, and H_2/CO Ratio

4.1.2.4 Moisture Content (MC)

Moisture content is another important design parameter, especially when estimating the energy requirement for drying process. High moisture content reduces biomass pyrolysis and increases drying requirement.

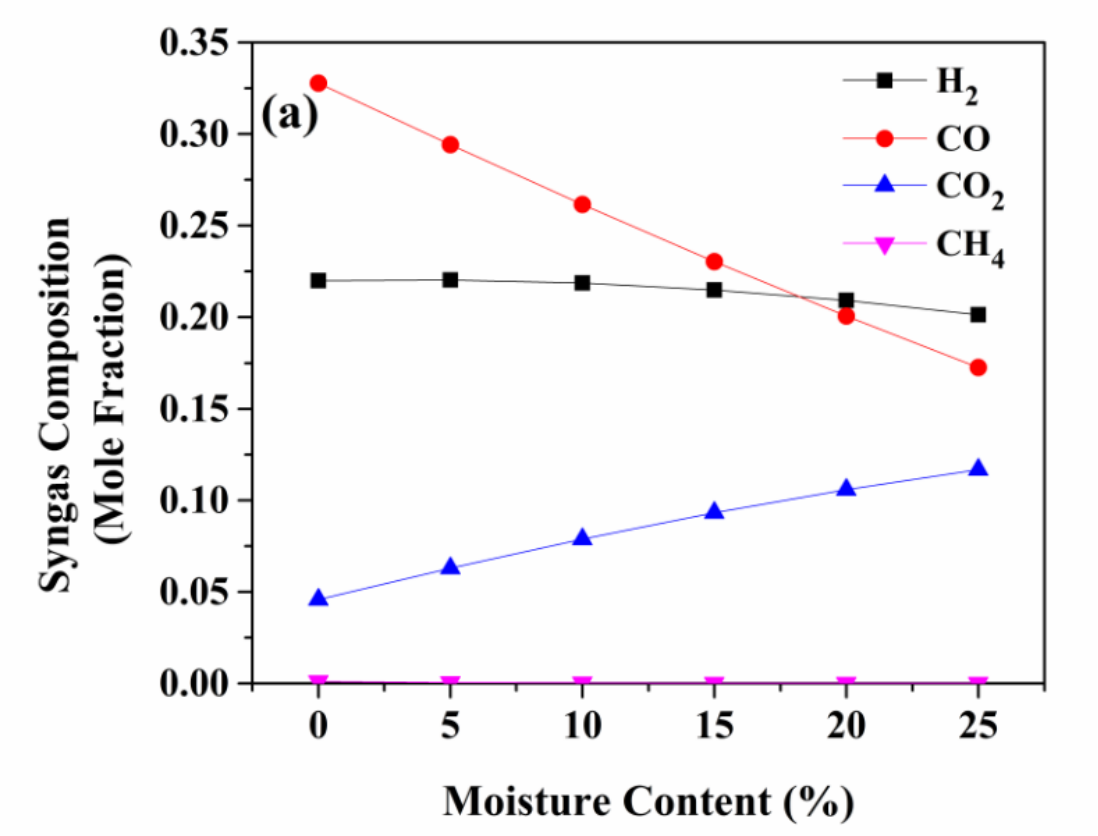

Figure 18. Moisture Content Vs Composition

It can be observed that with the increase in moisture content H_2 and CO concentration decreases, CO_2 increases and CH_4 remains constant. The decrease in CO concentration and increase in CO_2 could be because of water gas shift reaction which was enhanced by the increase in moisture content, one of the reactants in the reaction. The slight decrease in H_2 content could be because of the combined effect of all the reactions occurring in reduction as well as oxidation zone.

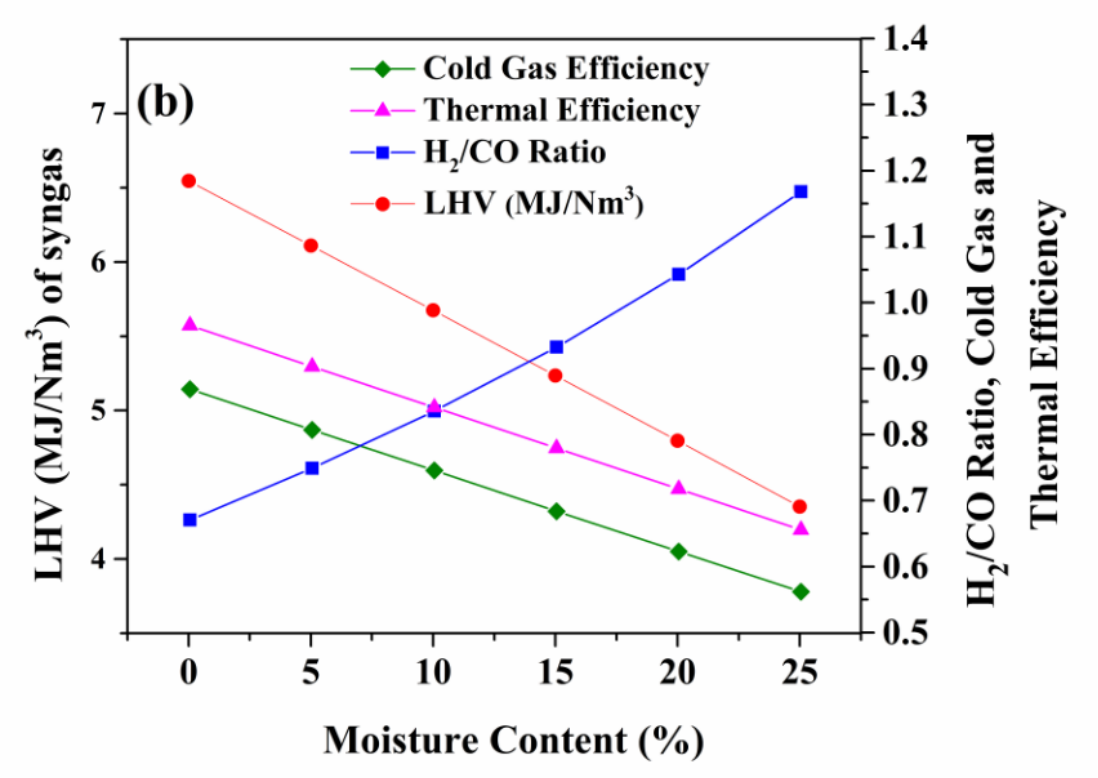

Figure 19. Moisture Content Vs LHV, CGE, H_2/CO Ratio

With the increase in MC H_2/CO ratio increases since H_2 concentration almost stays constant, but CO concentration decreases with the increasing MC. LHV of syngas decreases with the increase in MC because CO decreases with the increase in MC while H_2 and CH_4 do not vary with varying MC. CGE also decreases with decrease in LHV of syngas.

4.2 Solid Oxide Fuel Cell

4.2.1 Model Validation

The main façade of the Model was validation with the results from the published data for the SPGI 100 kW CHP SOFC stack operating on following syn-gas composition: 45.8% H_2, 21.6% CO, 10.0% CH_4, 21.2% CO_2, 1.4% N_2 (volume %, dry basis) and 25.7% H_2O (volume %, wet basis) [5]. The model inputs parameters were;

Table 13. SOFC Model input parameters

Parameters	**Values**
Operating Temperature (^OC)	910
Operating Pressure (Pa)	109431
Fuel Utilization Factor (UF) (%)	85
Air Utilization Factor (UA) (%)	16.7
DC – AC Efficiency (%)	92
Input Air Temperature (^OC)	630
Input Fuel Temperature (^OC)	300
Steam to Carbon Ratio (STCR)	2.5
Area (m^2)	96.0768

Simulation results were compared with the literature for power of 120 Kw.

Table 14. SOFC Model Validation

Parameters	**Literature**	**Our Model**
Current Density mAmp/cm^2	188.7	185.1
Cell Voltage (mV)	662	676
Gross Efficiency (%)	42.53	43.7
Net Efficiency (%)	37.04	36.83

4.2.2 Sensitivity Analysis

Validated model was run with the syngas from the gasifier modeling. Efficiency was calculated and sensitivity analysis by varying different design parameters were performed.

For power of 120 kW, following results were obtained.

Table 15. SOFC Results for 120 kW

Current Density (mAmp/cm^2)	197.6
Voltage (mV)	630
Syngas Flowrate (kmol/hr)	15.53
LHV of syngas (MJ/kmol)	70.85
Gross Efficiency (%)	36.3
Net Efficiency (%)	29.6

4.2.2.1 Current Density (ZJ)

One of the main parameters affecting SOFC's performance was current density. Current density was varied from 20 mAmp/cm^2 to 680 mAmp/cm^2. It was done by varying the mass flowrate. Current density increases with increase in biomass flowrate since increased flowrate, increase the amount of H_2 consumed, which results in more current and in turn more current density.

The Nernst voltage which is the ideal came out to be around 0.87 volts and remained almost constant with increase in ZJ. This is because, Nernst voltage depend on mole fractions, and operating temperature and pressures of SOFC but not on flowrate of biomass. Actual voltage however, constantly decreases with increase in current density because of the increase in voltage losses with ZJ.

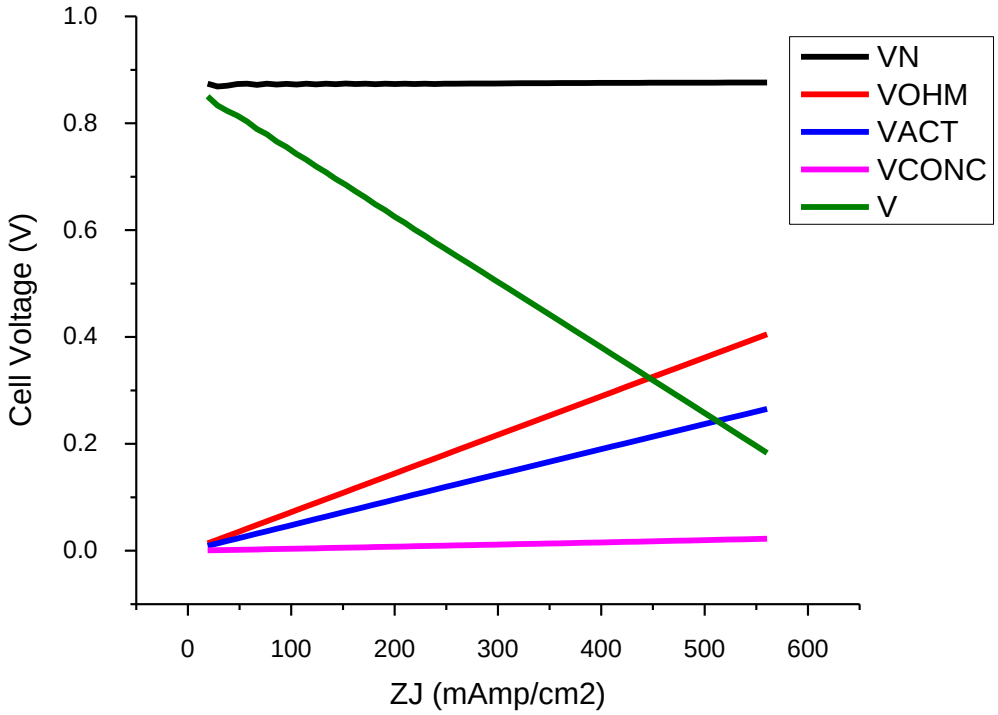

Figure 20. Current Density Vs Nernst Voltage, Voltage Losses and Actual Voltage

Graph shows ohmic loss increases more sharply with ZJ as compared to other losses. This is because ohmic loss is highest in case of tubular SOFC because of long current paths and from equation it can be seen that ohmic loss is directly proportional to current density, thus increased biomass flow will increase resistance to electrons and ions flow in long SOFC. Activation losses also increases with ZJ, but is less as compared to ohmic loss. It is the voltage loosed by reacting species when overcoming the energy barrier. It is less in SOFC because of high operating temperatures. Activation loss is calculated by multiplying resistivity terms with current density, thus the increase in activation loss with increase in ZJ. Concentration loss do not show a lot of change with increase in current density since it depends majorly on electrode properties and geometry.

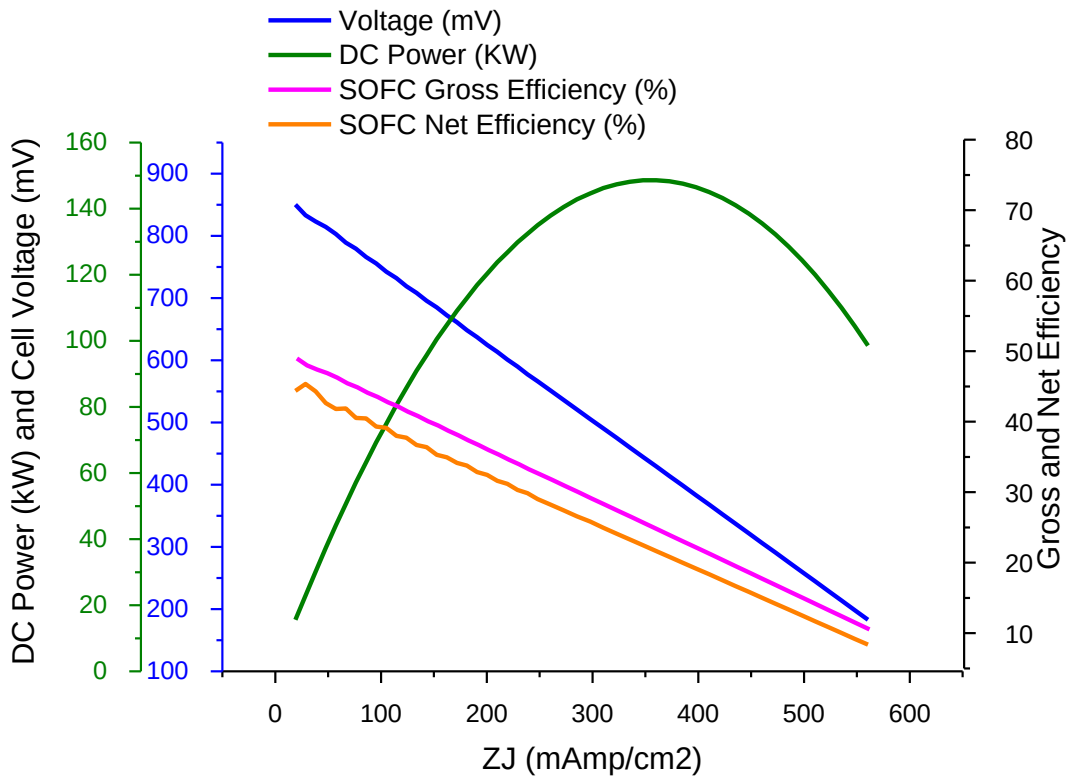

Figure 21. Current Density Vs Biomass Flowrate, Voltage, SOFC Gross and Net Efficiency

4.2.2.2 Steam to Carbon Ratio (STCR)

Current density increases with increase in STCR. This Increase in current density is because of increased syngas flowrate through SOFC. The fraction of H_2O in anode off-gas increases and H_2 and O_2 decreases as compared to gas entering SOFC. This increases the H_2 consumed which in turn increases the amount of current through it. Voltage and efficiency however decreases with increase in STCR. Decrease in voltage is because of decrease in Nernst voltage with increase in STCR. Increase in STCR decrease anode temperature because of increase in flowrate which is due to increased steam. Also, average H_2O mole fraction in anode-off gas increases with STCR, because of increased CH_4 reforming. In ideal voltage calculation, mole fraction of H_2O comes in denominator, while Anode temperature comes in numerator. Thus, decrease in Tanode and increase in H_2O mole fraction decreases voltage. Gross and net efficiency decreases because of increase in syngas flowrate to SOFC and higher parasitic power for increased flowrates of syngas and air.

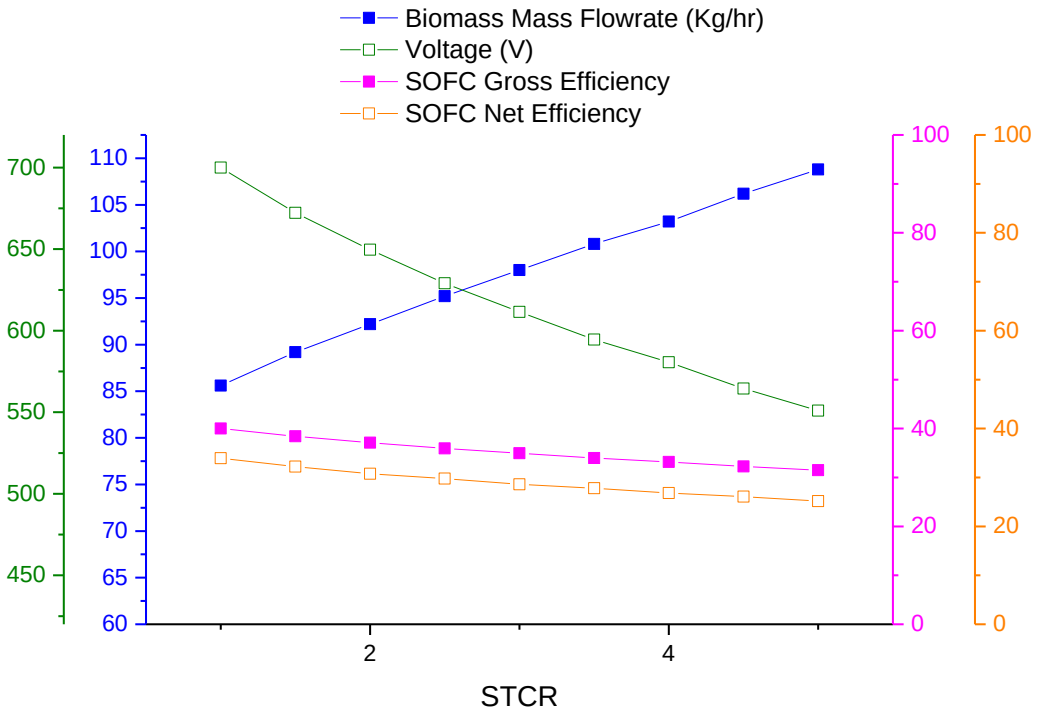

Figure 22. STCR Vs Biomass Flowrate, Voltage, SOFC Gross and Net Efficiency

4.2.2.3 Fuel Utilization Factor (UF)

Increasing the fuel utilization factor slightly increases the cell voltage, decreases fuel flowrate, and increases the efficiency and current density. Increase in UF increases the amount of H_2 consumed due to which more current is produced, hence the increase in current density. With increase in UF less syngas is required to produce the power of 120kW thus its flowrate decreases. Voltage decreases with increase in UF because of increase in losses. Efficiency however increases because of decrease in fuel requirement to achieve the required power output. Difference in gross and net efficiency accounts for the parasitic power.

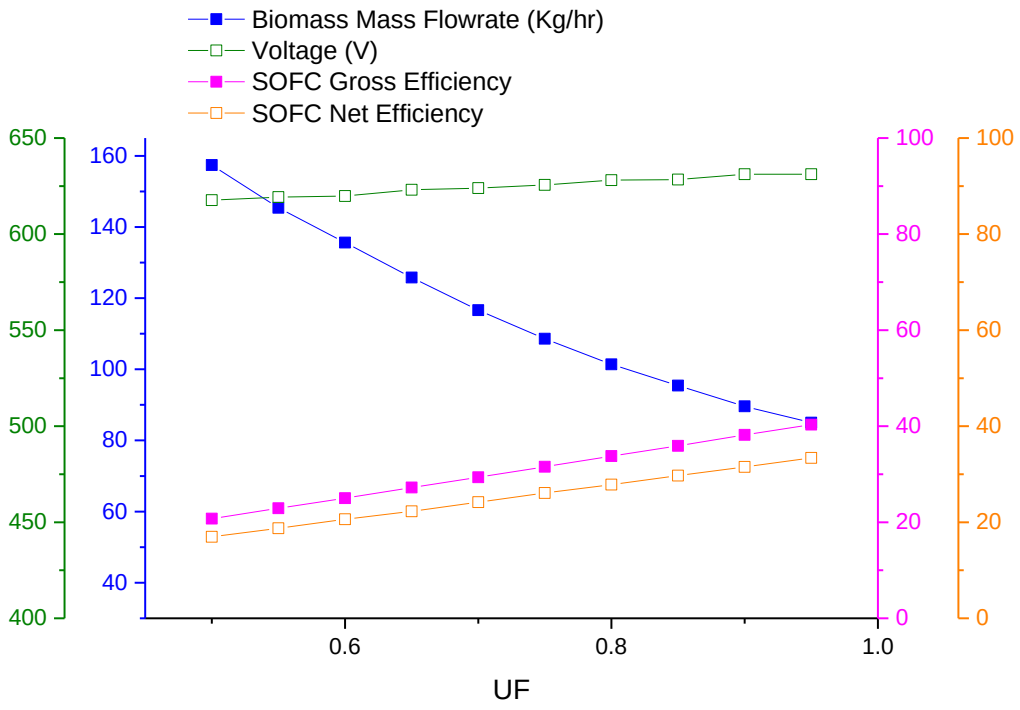

Figure 23. UF Vs Biomass Flowrate, Voltage, SOFC Gross and Net Efficiency

4.2.2.4 Air Utilization Factor (UA)

With the increase in air utilization factor air flowrate decreases drastically, biomass flowrate increases, cell voltage decreases while efficiency almost remain constant. Voltage change is between 600-640 mVolts. Decrease in voltage is because of the slight increase in voltage losses. Effect of air utilization factor on gross efficiency is very insignificant. However, net efficiency first increases sharply, and then almost become constant around 50% UA. Less net efficiency in the beginning is because of high air flowrate at low air utilization factor due to which parasitic requirement is also high. Decrease in air flowrate with increase in UA also reduces the parasitic requirement due to which net efficiency increases afterwards. Decrease in air flowrate is because of more utilization of oxygen in SOFC.

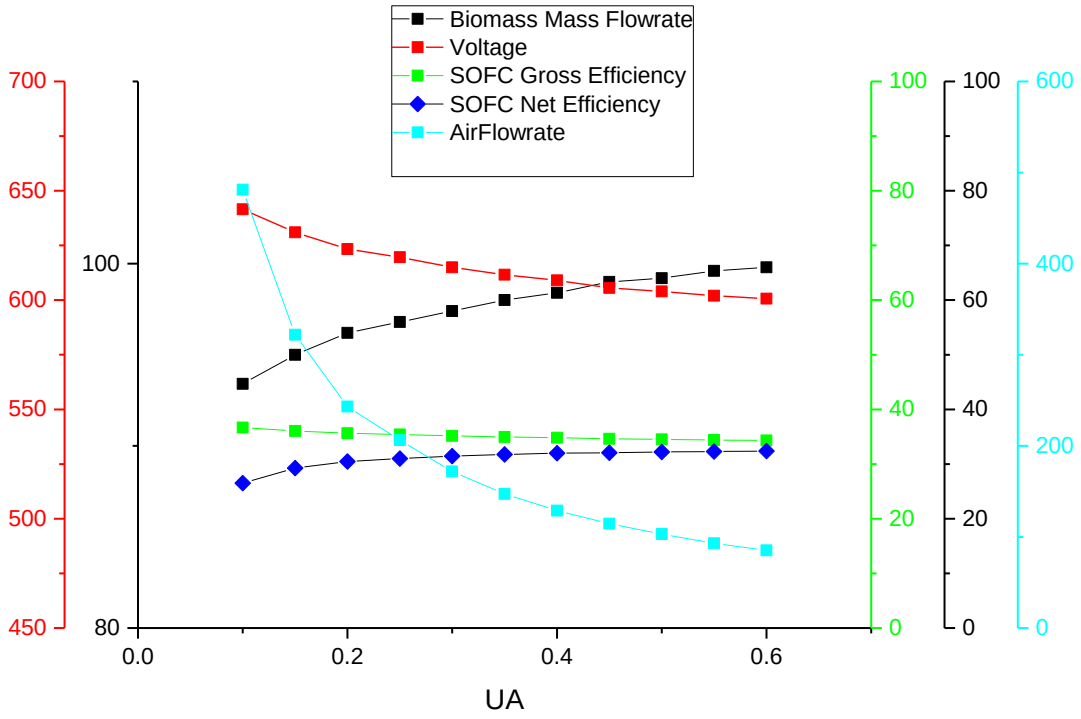

Figure 24. UA Vs Biomass Flowrate, Voltage, SOFC Gross and Net Efficiency

Summary

In this section, both the models for gasifier as well as SOFC were validated using the data from literature. Than sensitive analysis was performed for both the systems by varying different operating parameters. Efficiency of the systems were compared at different operating conditions.

References

[74] L. Wei, J. A. Thomasson, R. M. Bricka, R. Sui, J. R. Wooten, and E. P. Columbus, "Syn-Gas Quality Evaluation for Biomass Gasification with a Downdraft Gasifier," *Trans. ASABE*, vol. 52, no. 1, pp. 21–37, 2009.

[75] A. Gagliano, F. Nocera, F. Patania, M. Detommaso, and M. Bruno, "Evaluation of the performance of a small biomass gasifier and micro-CHP plant for agro-industrial firms," *Int. J. Heat Technol.*, vol. 33, no. 4, pp. 145–154, Dec. 2015.

[76] A. Gagliano, F. Nocera, F. Patania, M. Bruno, and D. G. Castaldo, "Comptes Rendus Chimie A robust numerical model for characterizing the syngas composition in a downdraft gasi fi cation process," *Comptes rendus - Chim.*, vol. 19, no. 4, pp. 441–449, 2016.

[77] Y. Lu, J. Hu, J. Han, and F. Yu, "Synthesis of gasoline-range hydrocarbons from nitrogen-rich syngas over a Mo/HZSM-5 bi-functional catalyst," *J. Energy Inst.*, vol. 89, no. 4, pp. 782–792, Nov. 2016.

[78] T. O. Somorin, S. Adesola, and A. Kolawole, "State-level assessment of the waste-to-energy potential (via incineration) of municipal solid wastes in Nigeria," *J. Clean. Prod.*, vol. 164, pp. 804–815, Oct. 2017.

[79] M. B. Nikoo and N. Mahinpey, "Simulation of biomass gasification in fluidized bed reactor using ASPEN PLUS," vol. 32, pp. 1245–1254, 2008.

[80] P. Mckendry, "Energy production from biomass (part 2): conversion technologies," vol. 83, no. July 2001, pp. 47–54, 2002.

[81] P. Lahijani, Z. Alimuddin, A. Rahman, and M. Mohammadi, "Bioresource Technology Microwave-enhanced CO 2 gasification of oil palm shell char," *Bioresour. Technol.*, vol. 158, pp. 193–200, 2014.

[82] J. J. Hernández, G. Aranda, J. Barba, and J. M. Mendoza, "Effect of steam content in the air – steam fl ow on biomass entrained fl ow gasi fi cation," vol. 99, pp. 43–55, 2012.

[83] L. E. Taba, M. Faisal, W. Ashri, M. Wan, and M. H. Chakrabarti, "The effect of temperature on various parameters in coal , biomass and CO-gasification : A review," *Renew. Sustain. Energy Rev.*, vol. 16, no. 8, pp. 5584–5596, 2012.

[84] M. Gabra, E. Pettersson, R. Backman, and B. Kjellstrom, "Evaluation of cyclone gasiÿer performance for gasiÿcation of sugar cane residue — Part 1 :

gasiÿcation of bagasse," vol. 21, pp. 351–369, 2001.

[85] Z. A. Zainal, A. Rifau, G. A. Quadir, and K. N. Seetharamu, "Experimental investigation of a downdraft biomass gasiÿer," vol. 23, no. May, pp. 283–289, 2002.

Chapter 5: Conclusion and Future Recommendations

5.1 Conclusion

Following conclusions were drawn from this study:

- A detailed four step downdraft gasification process is modelled. Oxidation and reduction zones are modelled using the Gibbs free energy minimization approach. All reactions reach equilibrium at the operating temperatures.
- Sensitivity analysis was performed by varying gasifying agent composition, reduction zone temperature, moisture content, and equivalence ratio. Syngas composition, and efficiency parameters were plotted against the varied operating parameters.
- From sensitivity analysis, for efficient gasification following conclusions were drawn; reduction zone should be operated between 700-1000 ^{O}C. Equivalence ratio should be set between 0.05-0.25. Moisture content should be till 10%.
- Cold gas as well as thermal efficiencies increased with increase in oxygen content in the gasifying agent.
- Carbon is left unconverted at low temperatures and low equivalence ratio's.
- A detailed solid oxide fuel cell was modelled using aspen plus simulator. Anode was modelled using RGibbs reactor. Cathode's function was to supply required oxygen to anode. Fortran blocks were used to perform calculations.
- Sensitivity analysis was conducted to check the influence of STCR, UA, UF, and Current Density on Biomass Flowrate, Voltage, SOFC Gross and Net Efficiency required to achieve 120 Kw power.
- Optimum steam to carbon ratio was found to be <1.
- Optimum air utilization factor was between 0.2 – 0.4.
- Optimum fuel utilization factor was around 0.8 – 1.

Chapter 6: Work done at Arizona State University

6.1 Solar Thermal Space Heating with Thermal Energy Storage

The first project I worked on was on Solar Space Heating system integrated with thermal energy storage. In this project a small system consisting of solar panels, solar thermal collectors, pcm and water container, battery, and tubings has been made.

Main Assembly

- Flat Panel Solar Water Heater
- Water glycol System to Exchange Heat
- Container for Phase Change Material Storage
- PV Module to operate pumps
- Pumps

For Analysis and Data Logging

- Thermocouples with temperature DataLogger
- Solar Rdiation, Ambient Temperature DataLogger
- Flowrate Controller

Softwares

- Hoboware(Temp, Radiation)
- OM-CP(Temperature Data Logger)

When I arrived, the system was already functional. My work on the system involved testing different pcm materials and calculating their charging and discharging rates. Charging and discharging rates were calculated under different conditions. Water glycol system was used as the working fluid which gets heated in the thermal collector, working fluid then transfers heat to the pcm(Wax and SAPA) which gets charged and then transfers heat to the water radiator unit, heating the water. Overall efficiency was also calculated for the system.

Following Calculation were Performed

- Energy Collected from Solar Collector
- Energy Stored During Charging
- Energy Stored During Discharging

- Energy Recovered through Radiator

6.2 Electrode Development for Water Splitting

The second project I worked on was on photo anode development for more efficient water splitting. Bismuth Vandate was doped with different concentrations of Erbium, tungsten and molybdenum to check the effect on charge separation and light absorption capabilities.

These 5 compositions were spin coated on Fluorine doped Tin Oxide(FTO) glass slides

- BiVO4
- 2% Mo-$BiVO_4$
- (2%Mo3%Er)$BiVO_4$
- (1.5%Mo0.5%W)$BiVO_4$
- (1.5%Mo0.5%W3%Er)$BiVO_4$

Solutions were prepared first using weighing machine and magnetic stirrer. Fluorine doped tin oxide slides were coated with these solutions using spray coating machines. Afterwards, copper wires were attached using silver adhesive and epoxy adhesive. Electrolyte was prepared by dissolving 1.743g potassium phosphate in 100 ml water. Potentiostat was used to measure photocurrent and UV-Visible Spectrophotometer was used to measure absorbance and transmittance. Results were plotted and analyzed on origin. Erbium doped Bismuth Vandate showed relatively better performance.

6.2.1 Electrochemical Studies using Potentiostat

Reference Electrode: Calomel Electrode

Counter Electrode: Platinum Electrode

Continuous Current Measurement (-1 - 2V)

- Front Side
- Back Side

Chop Light Measurement (-1 - 2V) (3 minutes gap)

- Front Side
- Back Side

Impedance Measurement

6.2.2 UV-Visible Spectrophotometer

- Absorbance Measurement
- Transmittance Measurement

Acknowledgment

All praise to the great **Allah Almighty** who has bestowed me with the opportunity to seek knowledge and enabled me to fulfil the obligation to explore the world of science up to my maximum limits.

I would like to express my sincere gratitude to my **research supervisor Dr. Muhammad Zubair** for his motivation, continuous support, patience and immense knowledge. He guided me completely through-out my research work. Working under his supervision has indeed broadened my vision.

I am also really thankful to my GEC members, **Dr Naseem Iqbal, Dr. Rabia Liaquat and Dr. Iftikhar Ahmed** for sparing precious time from their busy schedules, for guidance, suggestions, as well as moral support. Besides this I would like to thank the USPCAS-E faculty for being really cooperative. A special thanks to my friends all over the globe.

Last but not the least, I would like to pay my regards to my family for their un-parallel love, encouragement and support throughout my research work.

Annex- Research Paper

Parametric analysis of a steady state equilibrium-based biomass gasification model for syngas and biochar production and heat generation

Wajeha Tauqir*, Muhammad Zubair, Hassan Nazir
US-Pakistan Center for Advanced Studies in Energy (USPCAS-E), National University of Sciences and Technology, Islamabad 44000, Pakistan

Abstract
In this study, a comprehensive steady-state model of downdraft biomass gasification process was developed using Aspen Plus simulation software. All four major gasification zones: drying, pyrolysis, oxidation, and reduction were modeled separately. Oxidation and Reduction zones were modeled using the Gibbs free energy minimization method with restricting chemical equilibrium approach. The simulated model was compared with the results of a wood-fed downdraft gasifier studied by Wei et al. and showed a root mean square error of 2.53. A parametric analysis was performed to analyze the effect of the gasifying agent, gasification temperature, equivalence ratio, and moisture content on the performance of gasifier. Performance evaluation of gasifier for syngas production and heat generation was performed by determining the low heating value of syngas, cold gas efficiency and thermal efficiency. The results indicated that the Equivalence ratio (ER) is the most important factor in gasification. Changes in the ER shows a very significant variation in syngas composition. Moreover, the increase in cold gas and thermal efficiencies was also very prominent until 700 ºC after which it becomes constant. Biochar production was possible below 700 ºC and 0.14 ER.

Keywords: Gasification; Thermal Efficiency; Low Heating Value; Aspen Plus; Biochar
*Corresponding author: Email: 16esewajeha@uspcase.nust.edu.pk, wajeha.tauqir8@gmail.com

1. Introduction

Fossil fuels, have the largest share in today's world energy supply and will contribute to 80% of the world's energy supply mix by 2040 if continued at the same pace [1,2]. This scenario will lead to disastrous consequences in terms of environmental damage because of greenhouse gas emissions associated with fossil fuels. Biomass is considered as one of the most promising renewable energy sources and has the potential to replace fossil fuels [3]. Biomass a carbon neutral fuel also mitigates a very common problem in most other renewable energy sources; such as the intermittent nature of wind and solar energy. Bioenergy is estimated to contribute between a quarter and third of the global energy supply mix by 2050 [4]. Biomass to bio-energy conversion can be divided into two major categories; biochemical and thermochemical [5,6]. Thermochemical conversion is more efficient as compared to biochemical particularly for syngas production [7]. There are several thermochemical routes of biomass conversion into a useful product, depending upon the characteristics of feedstock and the required end-product. Thermochemical conversion routes for bioenergy production are shown in Table 1, and gasification particularly has the highest conversion efficiency among the other conversion techniques [8,9].

Thermochemical Processes	Products	Applications
Gasification	Syngas	Electricity and heat generation and methanol production
Pyrolysis	Charcoal, Liquids, Gases	Chemicals extraction, upgradation to diesel, electricity, bio char
Liquefaction	Liquids	Bio chemicals and diesel production, electricity
Combustion	Heat	Electricity generation

Table 1. Thermochemical conversion routes for biomass to bioenergy

Biomass gasification to produce syngas (a mixture of CO and H_2) is one of the major application of gasification process. Produced syngas can be used in the synthesis of various other chemicals such as Fischer-troph fuels and ammonia [10]. Syngas can also be used as a fuel in internal combustion engines and fuel cells [11]. In order to access different gasification schemes and their performances, Aspen Plus Simulator has gained a lot of popularity among design engineers and researchers. It has been used by researchers to simulate processes for biomass-derived hydrogen production [12–15], syngas production [16–18] and for methanol synthesis [19,20]. Mathieu and Dubuisson [3] modeled the wood gasification process and found out that the injection of steam degrades thermal efficiency, and the optimum gasification efficiency is obtained at the oxygen factor of 25%. Begum et al. [21] analyzed the performance of an integrated fixed bed gasifier using different biomass feedstock such as wood waste, municipal solid wastes, and green wastes. Gasification temperature of 650 ^{o}C and air to fuel ratio of 0.3 were found to be optimum conditions for the three feedstocks. Dejtrakulwong et al. [22] modeled the downdraft gasification process and analyzed the effect of moisture content and air-to-fuel ratio on the gasification temperature and height of different zones. Gagliano et al. [23] developed an equilibrium based gasification model and validated it with the two experimental results. An average error of 15% was found with reference to the composition of product gas and less than 7% for the LHV predictions.

Though models for biomass gasification were developed using Aspen Plus, very few literatures report separate models for oxidation and reduction zones. Moreover, biochar production as a by-product was also neglected in those models. The purpose of this study is to develop all four stages of biomass gasification and perform parametric analysis to evaluate the effect of different operating parameters; gasifying agents, gasification temperature, equivalence ratio (ER), and moisture content (MC) on the syngas composition, low heating value (LHV), cold gas efficiency (CGE) and thermal efficiency. Bio-char production as a by-product is also evaluated during the analysis.

1.2. Biomass Gasification

Biomass Gasification is the thermochemical conversion of solid/liquid fuels into gaseous and solid products. Gasification principle is illustrated in Figure 1 [24–27].

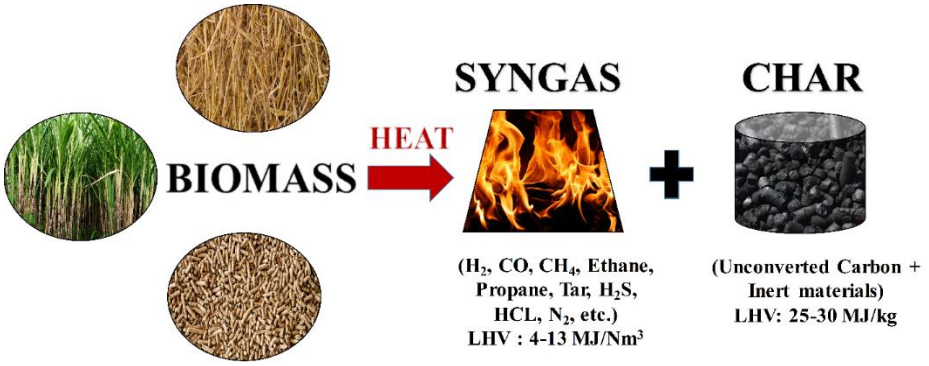

Figure 1. Gasification Principle

Downdraft biomass gasification process is divided into four main stages; drying, pyrolysis, oxidation, and reduction. Oxidation step provides heat energy to derive the gasification process [28,29]. Figure 2 shows the main processes involved in a fixed bed downdraft biomass gasifier [30].

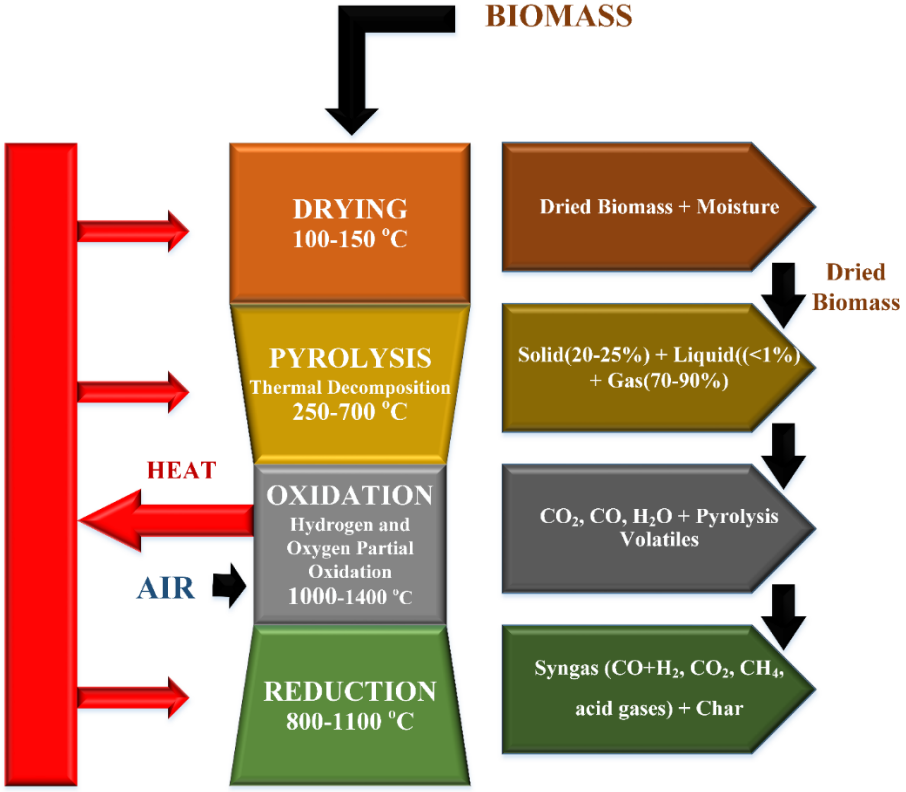

Figure 2. Overview of Biomass Gasification Process

Drying is the first step of gasification, in which the moisture content of biomass feedstock is reduced to a certain amount by supplying heat. Then in the pyrolysis zone, thermochemical decomposition of the carbonaceous material into lower molecular weight compounds occur in the absence of oxygen. Reactions taking place below 300 °C are endothermic while those above 300 °C are exothermic. At the partial oxidation stage, heterogeneous reactions take place between solid carbonaceous fuel and oxygen, to produce CO_2 and a substantial amount of heat. Hydrogen also reacts with oxygen to form H_2O [31–33]. Subsequently, in the reduction zone, a number of chemical reactions take place at relatively high temperature to produce syngas (mainly CO and H_2) with high heating value (HHV). Main gasification reactions modeled in this study are given in Table 2.

	Chemical Reaction	Heat of Reaction (kJ/mol)	Reaction Name	Reaction Number
Drying				
	Moist Feedstock + Heat → Dry Feedstock + H_2O	NA	Drying	R1
Pyrolysis				
	Dry Feedstock + Heat → Char + Volatiles	NA	Thermal Decomposition	R2
Partial Oxidation				
	$C + O_2 \rightarrow CO_2$	-393	CO Oxidation	R3
	$2H_2 + O_2 \rightarrow 2H_2O$	-242	H2 oxidation	R4
Reduction				
	$C + CO_2 \leftrightarrow 2\ CO$	+172	Boudouard Reaction	R5
	$C + H_2O \leftrightarrow CO + H_2$	+131	Water gas Reaction	R6
	$CO + H_2O \leftrightarrow CO_2 + H_2$	-41	Water gas shift Reaction	R7
	$C + 2H_2 \leftrightarrow CH_4$	-74	Methanation Reaction	R8
	$CH_4 + H_2O \leftrightarrow CO + 3H_2$	+206	Steam Methane Reforming	R9

Table 2. Chemical reactions involved in the process

2. Modeling Downdraft Gasifier

In this study, biomass gasification processes in a downdraft gasifier are modeled using Aspen Plus V10 simulator. Aspen Plus allows simulating chemical engineering processes using inbuilt process models. First of all, process flowsheet was made utilizing inbuilt unit operation blocks. Then their property method, and initial and operating conditions were specified. Fortran blocks were used to model operations not present in Aspen Plus library.

2.1. Property Method

Peng Robinson equation of state with the Boston-Mathias alpha function (PR-BM), was specified as the property method to calculate thermodynamic properties of the components [34]. PR-BM is used for processes involving, nonpolar and mildly polar mixtures such as light gases and hydrocarbons. Units were set to METSOLIDS, metric system units. All the components in the process were then specified as conventional components except for Biomass and Ash which were specified as Non-Conventional (NC). For NC components, enthalpy calculation model was set to HCOALGEN, and density to DCOALIGT [35]. In the simulation mode, the stream class was set to MIXCINC, here "MIX" represents mixed sub-stream, "CI" represents CISOLID, and "NC" represents nonconventional components.

2.2. Flowsheet Development

Process flowsheet of biomass to syngas production route with requirements of Fortran subroutines and reactions, mentioned is shown in Figure 3.

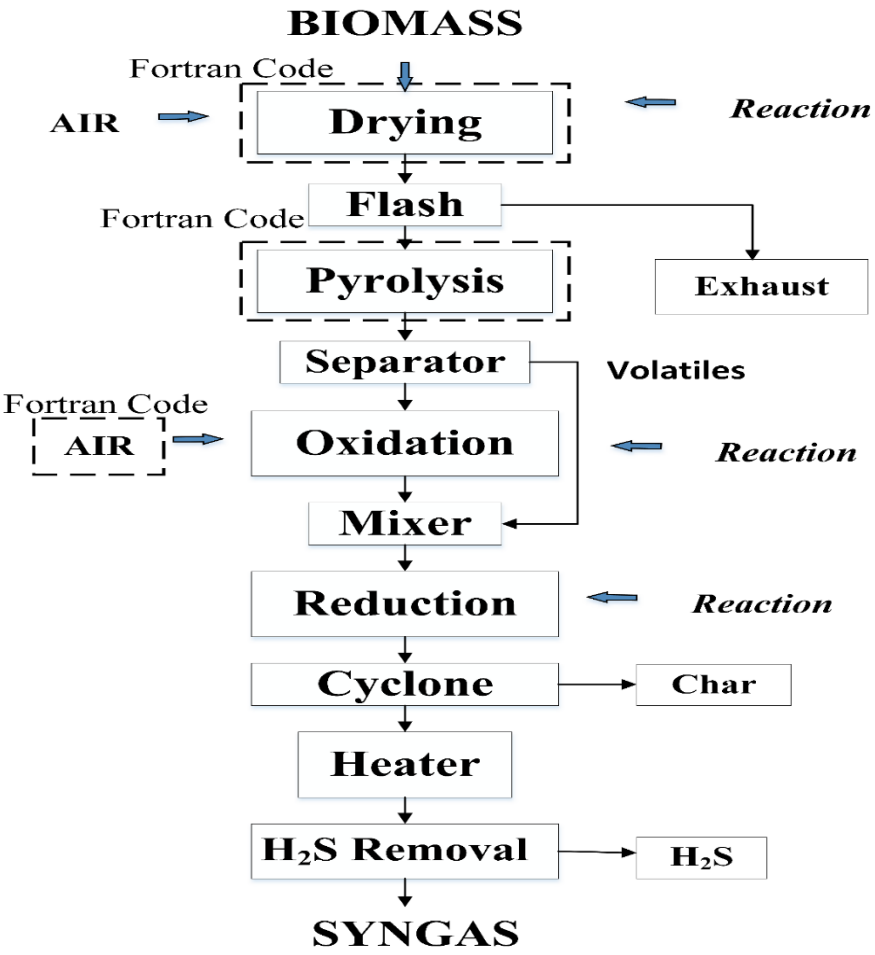

Figure 3. Process flowchart of downdraft gasifier model

Main Assumptions:

1. The whole process is steady-state and isothermal.
2. Heavy hydrocarbons are not considered.
3. Ash is considered to be inert.
4. Blocks are zero-dimensional and have a uniform temperature.
5. Residence time is long enough to reach equilibrium in the R-Gibbs block.
6. The particle size distribution of biomass is not considered.
7. No NOx, SOx are produced. Only NH3 and H_2S are formed.

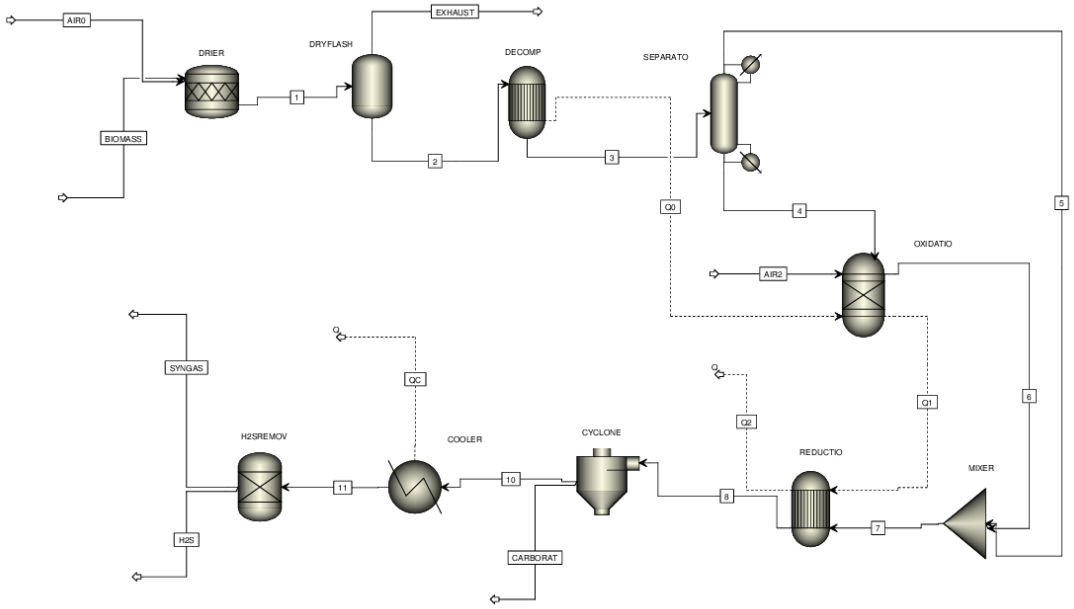

Figure 4. Process flowsheet for downdraft biomass gasification in Aspen Plus

"BIOMASS" stream defined as NC stream with proxanal, ultanal, and sulfanal attributes defined was introduced in the "DRIER" block. Air at atmospheric pressure and temperature was entered in the "Drier" block through the stream "AIR0" to provide heat for the drying process. The Rstoic block was used to convert a portion of biomass into water. The following reaction was specified in the Rstoic block to model the conversion process.

biomass (wet) → 0.0555084 H_2O (R10)

According to (R10), 1 mole of biomass reacts to form 0.0555084 moles of water. Fractional conversion of biomass was controlled using a calculator block. The mixture then enters the "DRYFLAS" block which separates the dried biomass from the exhaust. Dried biomass then goes to the "DECOMP" block which simulates the pyrolysis process. RYield unit operation model was used for this purpose [36]. Component yields were calculated using a Fortran calculator block which takes into consideration the ultimate analysis of the biomass feedstock [37]. Decomposed yield then enters the "SEPARAT" block, which separates the char and hydrogen from other volatiles. Char and hydrogen stream go to oxidation block modeled using RGibbs unit operation block. Restrict chemical equilibrium approach was selected and oxidation reactions identified in Table 2 were specified in the block. Required oxygen was also provided by introducing an air stream. Its flow rate was set using a calculator block. Products of the oxidation block were mixed with the volatiles stream from "SEPARAT" block in "MIXER" and then entered in the "REDUCTIO" block. RGibbs reactor which calculates equilibrium using the Gibbs free energy minimization method was selected. Reduction reactions mentioned in Table 2 were specified in this block with the temperature approach option selected [38]. The product stream from "REDUCTIO" block called syngas then undergoes the syngas clean-up unit. "CYCLONE" separate solids from syngas. "COOLER" cools the syngas to around 300 ºC, to be used in bag filters, "H2SREMOV" in our flowsheet, to separate acid gases from syngas. Figure 4shows the process flowsheet in Aspen Plus. A summary of the blocks used in the flowsheet is shown in Table 3.

User ID	Aspen Plus ID	Description

DRIER	RStoic	Reduces the moisture content of the biomass feedstock
DRYFLASH	Flash2	Separates the moisture stream from dry biomass
DECOMP	RYield	Decompose the biomass into its components based on ultimate and proximate analysis. Operates at 500 ^{o}C and 1.01325 bar.
SEPARATO	Sep2	Separates the volatiles from char
OXIDATIO	RGibbs	Oxidation of Char (carbon) occurs in this block. Operates at 950 ^{o}C and 1.01325 bar.
MIXER	Mixer	Oxidation products are mixed with the separated volatiles
REDUCTIO	RGibbs	Reduction of mixed stream occurs which produces syngas. Operates at 789 ^{o}C and 1.01325 bar.
CYCLONE	SSplit	Separates unreacted carbon from syngas
COOLER	Heater	Reduces the temperature of syngas to 300 ^{o}C.
H2SREMOV	Sep	Separates out H_2S from syngas

Table 3. Description of unit operation blocks used in this simulation and their operating conditions

2.3. Efficiency Calculations

In order to access the performance of gasification model, syngas low heating value (LHV), cold gas efficiency (CGE), thermal/hot gas efficiency (HGE), and H_2/CO ratios were calculated.

Low heating value is calculated using the following formula;

$$LHV(MJ\ /\ 〖Nm〗\text{^}3) = X\_H2 * 〖LHV〗\_H2 + X\_CO * 〖LHV〗\_CO + X\_CH4 * 〖LHV〗\_CH_4 \quad (1)$$

where X_ H_2, X_CO, and X_ CH_4 are the volume fractions of hydrogen, carbon monoxide and methane in the syngas, respectively.

Standard heating values of H_2, CO, CO_2, and CH_4 are given in Table 4;

Gases	**H_2**	**CO**	**CO_2**	**CH_4**
HHV (MJ/Nm^3)	12.74	12.63	0	39.82
LHV (MJ/Nm^3)	10.78	12.63	0	35.88

Table 4. Standard heating values of H_2, CO, CO_2, and CH_4

Cold gas efficiency (CGE) determines the energy which is transferred from biomass to syngas. It can be calculated using Eq. (2);

$$CGE = \frac{(MF_{syngas} * LHV_{syngas})}{(MF_{biomass} * LHV_{biomass})} \quad (2)$$

In Eq. (2), MF and LHV give the flow rate and low heating value of the respective subscripts. It is called cold gas efficiency as it does not take into account the temperature of the gas leaving the gasifier. Higher the CGE, higher the carbon conversion.

Thermal/Hot Gas efficiency (HGE) takes into account the sensible heat content of the syngas leaving the gasifier. It is calculated when the syngas produced is to be used for direct combustion or in internal combustion engines for electricity production.

$$HGE = \frac{(LHV_{syngas} * \dot{V}_{syngas}) + (C_{p,syngas} * \dot{V}_{syngas} * \rho_{syngas} * \Delta T)}{LHV_{biomass} * \dot{m}_{biomass}} \quad (3)$$

where, LHV is the low heating value of the respective subscripts. $\dot{m}$_biomass gives the mass flow rate of biomass. C_(p,syngas) is the specific heat capacity, $\dot{V}$_syngas is the volumetric flow rate and ρ_syngas is the density of syngas.

3. Results and Discussions

3.1. Model Validation

The simulated biomass gasification model was validated using the experimental data conducted by Wei et al. [39] on hardwood chips fed pilot scale downdraft gasifier using air as the gasifying agent. Experimental Run # 14 was selected to validate the model. Operating parameters for this experimental run are given in Table 5. Ultimate and proximate analysis (dry basis) of hardwood chips used in the study is given in Table 6.

Parameters	**Value**
Biomass Feeding Rate (kg/hr)	20.58
Operating Temperature (^oC)	850
Moisture Content (%)	10
Equivalence Ratio	0.254

Table 5. Operating parameters for the experimental run # 14 [39]

Equivalence ratio is given by Eq. (4).

$$ER = \frac{actual\ air/biomass\ ratio}{stoichiometric\ air/biomass\ ratio} \quad (4)$$

The equivalence ratio is further adjusted by the relation proposed by Gagliano et al. [40,41], according to it;

ER=0.008*M.C+0.1.047 (5)

where, M.C is for moisture content. This correlation in Eq. (5) is used to mitigate the problem of low CH_4 concentrations in thermodynamic equilibrium models of gasification [42].

Ultimate Analysis (wt. %)						**Proximate Analysis (wt. %)**			**Moisture (wt. %)**	**HHV (MJ/kg)**
C	H	O	N	S	Ash	VM	FC	Ash		
49.817	5.556	43.425	0.078	0.005	1.119	79.85	19.031	1.119	25	18.58

Table 6. Ultimate and Proximate Analysis

A comparison has been made of the predicted syngas composition and the LHV obtained from the simulated downdraft gasification model with the Wei et al. [39] experimental data on pilot scale downdraft gasifier. Figure 5 shows the comparison results. To evaluate the model results deviation from the experimental data is calculated by the root mean square (RMS) error, given by Eq. (6);

$$RMS = \sqrt{\frac{\sum_{i=1}^{N}(Y_{i,exp} - Y_{i,model})^2}{N}} \quad (6)$$

The developed gasification model showed an RMS error of 2.5326 from experimental data. It is evident that this model is in good agreement with the experimental data. The

predicted H_2 and CO yields were slightly higher than those reported by Wei et al.. Higher yields of these two could be because higher hydrocarbons production and tar gasification were neglected in this simulated gasification model. Predicted LHV was lower than the experimental results. This could be because of the low estimation of methane in simulated gasification model. Low methane concentration can be attributed to the fact that difference exists between real gasification system and modeled gasifier [45].

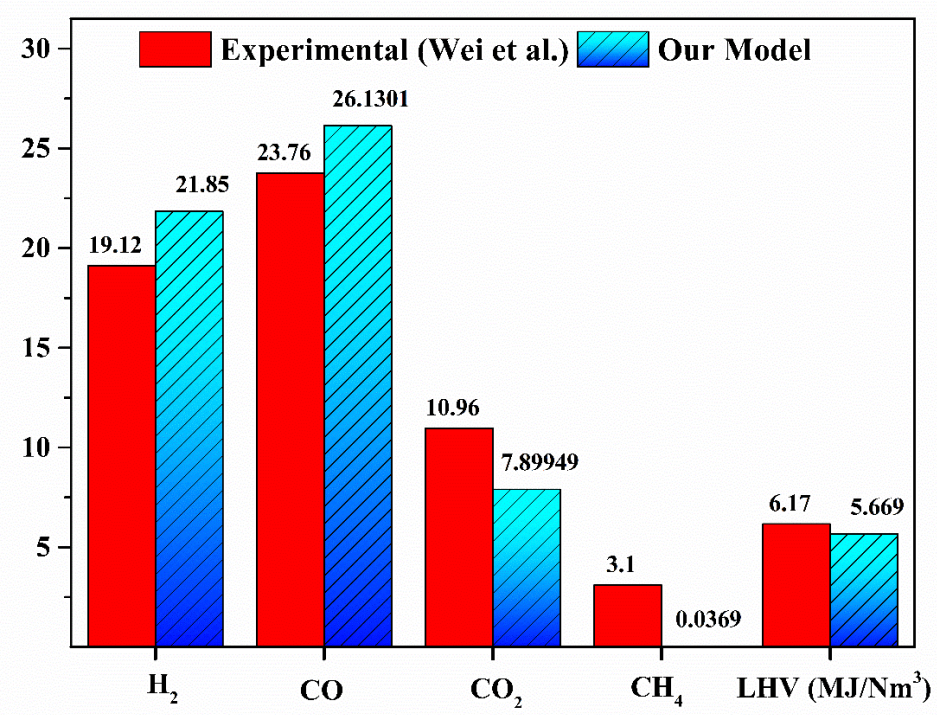

Figure 5. Comparison of Experimental results and Model predictions

The validated model was used to analyze the effect of varying different operating parameters on syngas composition, LHV, H_2/CO ratio, cold gas efficiency, and thermal efficiency. Operating parameters varied were; gasifying agent, gasification temperature (reduction zone), equivalence ratio, and moisture content of the feedstock. Effect of these parameters on biochar production was also evaluated.

3.2. Effect of Gasifying Agent

Comparison of different gasifying agents based on the predicted syngas composition and LHV of syngas is incorporated in Table 7. Gasifying agents compared were; air, enriched air, and pure oxygen. It can be observed that with the increment of O_2 % in gasifying agent, H_2 and CO content in syngas increases. This is because increased O_2 enhances the oxidation reactions, products of which further enhances the boudouard and water gas reactions. LHV increases with the production of CO, and H_2. Thus, LHV also increases with an increase of O_2 % in the gasifying agent.

	Mole Fraction				LHV (MJ/Nm^3)
	H_2	CO	CO_2	CH_4	
Air	0.2186	0.2613	0.0790	0.00034	5.669
Enriched Air (O_2: 50% + N_2:50%)	0.3031	0.3628	0.1104	0.00098	7.884
Pure Oxygen	0.3524	0.4222	0.1289	0.00153	9.187

Table 7. Effect of gasifying agents on composition and LHV of syngas

3.3. Effect of Gasification Temperature

Effect of gasification temperature on syngas composition was analyzed by varying it from 500 to 1000 ^{o}C. Figure 6a shows the variation in syngas composition with the increasing temperature. H_2 and CO concentration increases with the increase in temperature, and CO_2 and CH_4 concentration decrease with the increase in temperature. The increase in CO and H_2 concentration from 500 to 700 ^{o}C was because of the combined effect of boudouard, steam methane reforming and water gas reaction. These reactions are endothermic in nature and thus are favored with increasing temperature. The decrease in CO_2 and CH_4 concentration with increasing temperature was because of the exothermic nature of water gas shift and methanation reaction, making them unfavorable at higher temperatures. The decrease in H_2 concentration after 700 ^{o}C can be attributed to the combined effect of all the reactions occurring in the reduction zone. At low temperatures, water gas shift reaction contributed to hydrogen production, but this reaction was hindered at high temperatures. At high temperatures, water gas and steam methane reforming reactions contributed majorly to H_2 production, but steam methane reforming reaction was limited by the absence of reactants such as CH_4 at a higher temperature. From these observations, it can be concluded that water gas shift reaction majorly controls the H_2 production. The decrease in CO_2 concentration with the increase in temperature can be caused by the boudouard reaction which utilizes CO_2 to produce CO and being endothermic in nature is favored at high temperatures. CH_4 produced in methanation reaction was favored at low temperature because of its exothermic nature. Thus, the decrease in CH_4 concentration with an increase in temperature.

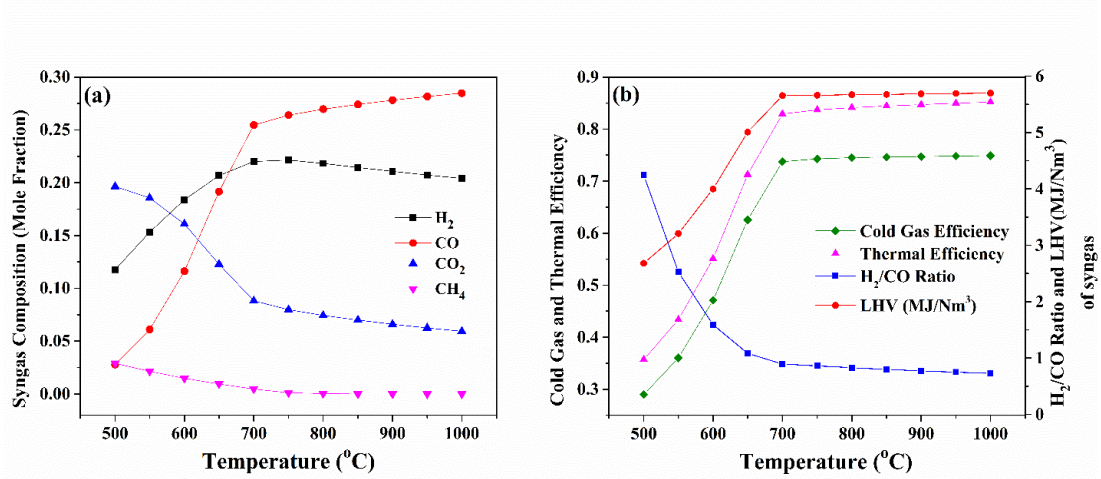

Figure 6. Effect of gasification temperature on (a) syngas composition. (b) syngas LHV, H_2/CO ratio, Cold gas and Thermal Efficiency

Figure 6b shows the variation in Cold gas efficiency, thermal efficiency, LHV of syngas, and H_2/CO ratio with increasing gasification temperature. Cold gas efficiency and LHV first increased abruptly from 26% at 500 ^{o}C to 57% at 700 ^{o}C and then almost became constant. H_2/CO ratio decreased sharply from 4.5 at 500 ^{o}C to 0.7 at 700 ^{o}C and then decreased slightly till 1000 ^{o}C. The decrease in H_2/CO ratio was because of an abrupt increase in CO concentration till 700 ^{o}C. After 700 ^{o}C, the increase in CO was very less, due to which the decrease in H_2/CO ratio was also very small. LHV increased till 700 ^{o}C because of increase in H_2, CO, and CH_4 concentrations. After 700 ^{o}C, LHV did not vary much because of decreasing H_2 concentration and slightly increasing CO concentration. CGE also followed the LHV trend as it is the main factor affecting the cold gas efficiency of the gasifier. Thermal efficiency which also takes into account the sensible energy stored in syngas, first increased and then became

constant, but is higher than cold gas efficiency, because it takes into account the increasing syngas temperature.

3.4. Effect of Equivalence Ratio (ER)

Effect of equivalence ratio on syngas composition and gasification performance was analyzed by varying it from 0.01-0.48. It can be observed in Figure 7a that H_2 and CO concentration decreased with an increase in ER, while CO_2 and CH_4 concentration increased with an increase in ER. ER is increased by increasing the oxygen supply in the oxidation zone. Increased oxygen supply enhances carbon and hydrogen oxidation reaction. These two reactions utilize carbon and hydrogen to produce CO_2 and H_2O. CH_4 production was very low because reactants of methanation reaction were consumed in hydrogen and carbon oxidation reactions.

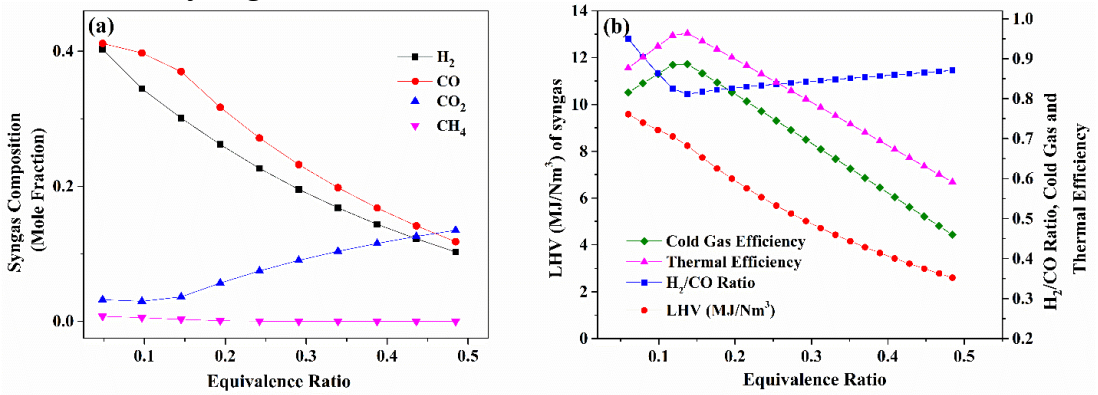

Figure 7. Effect of varying equivalence ratio on (a) syngas composition. (b) syngas LHV, H_2/CO ratio, Cold gas and Thermal Efficiency

Effect of ER on H_2/CO ratio, cold gas efficiency, thermal efficiency, and LHV was plotted in Figure 7b. It can be observed that the H_2/CO ratio first decreases and then increases with an increase in ER. This may be because at low ER, CO concentration was higher as compared H_2. With increasing ER, CO decreases while H_2 increases due to which H_2/CO ratio starts to increase after ER = 0.13. LHV of syngas decreased from 9.5 at ER = 0.06 to 2.6 at ER = 0.48. The decrease in LHV value was because of the decrease in H_2, CO, and CH_4 concentrations. Cold gas efficiency first increases until ER = 0.13 and then decreases until ER = 0.48. This is because in the beginning LHV was high but decreased rapidly with increasing ER. Thermal efficiency was higher than the cold gas efficiency because it takes into account the temperature of syngas coming out of gasifier.

3.5. Effect of Moisture Content

Effect of moisture content on gasification performance was studied by varying it from 0 to 25%. Figure 8a shows the effect of moisture content on syngas composition. It can be observed that with the increase in moisture content H_2 and CO concentration decreases, CO_2 increases and CH_4 remains constant. The decrease in CO concentration and increase in CO_2 could be because of water gas shift reaction which was enhanced by the increase in moisture content, one of the reactants in the reaction. The slight decrease in H_2 content could be because of the combined effect of all the reactions occurring in reduction as well as oxidation zone.

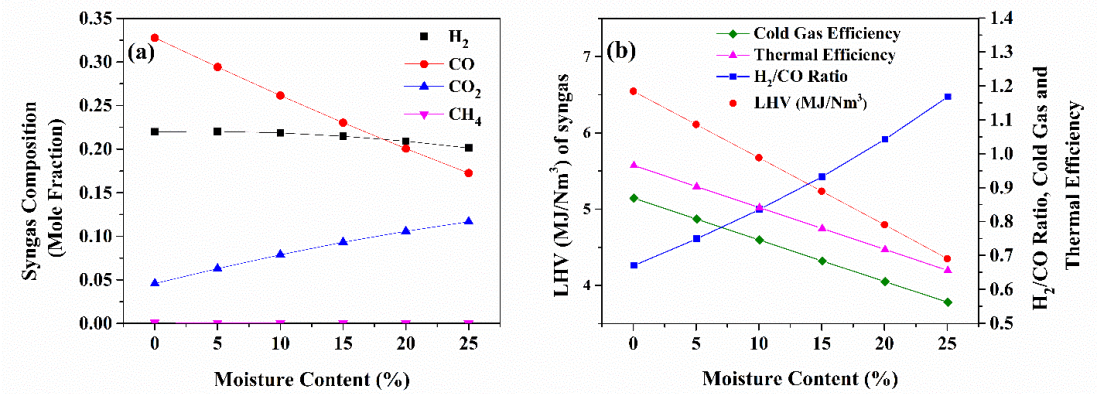

Figure 8. Effect of varying moisture content on (a) syngas composition. (b) syngas LHV, H_2/CO ratio, Cold gas and Thermal Efficiency

Figure 8b shows the effect of moisture content on H_2/CO ratio, cold gas and thermal efficiency, and LHV. It can be observed that with the increase in MC, H_2/CO ratio increases while cold gas efficiency, thermal efficiency, and LHV decreases. H_2/CO ratio increases because H_2 almost remains constant while CO concentration decreases abruptly. LHV of syngas decreases because CO decreases with the increase in MC. CGE also decreases with the decrease in LHV of syngas. Thermal efficiency showed a constant decrease because an increase in MC reduces the temperature of syngas.

3.7. Biochar (Unconverted Carbon) generation from the gasification model

Biochar is the by-product of the gasification process and it comprises of unconverted carbon. Effect of gasification temperature, moisture content, and equivalence ratio on biochar production was evaluated. Only gasification temperature and equivalence ratio affected the biochar production. Figure 9a shows the change in the amount of unconverted carbon with increasing temperature. It can be observed that the amount of unconverted carbon decreases with increase in temperature and becomes zero at 700 ^oC. The reason for this could be the combined effect of boudouard and water gas reactions that convert carbon into carbon monoxide. They are endothermic and are favored at high temperatures.

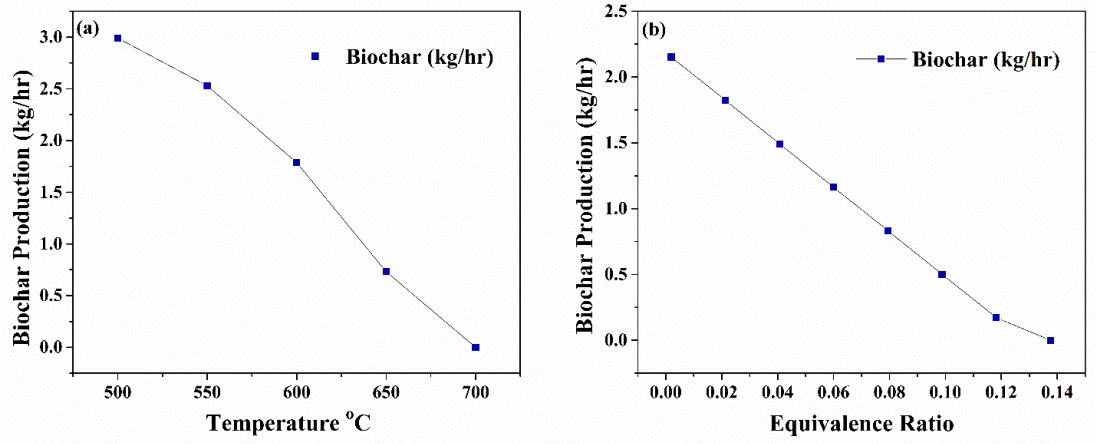

Figure 9. Biochar production (kg/hr) w.r.t (a) temperature (^oC). (b) equivalence ratio

Effect of Equivalence ratio on unconverted carbon is shown in Figure 9b. It can be observed that with the increase in equivalence ratio amount of unconverted carbon decreases and becomes zero around ER = 0.14. The reason for this recession in unconverted carbon with ER could be the availability of more O_2 to convert C into CO_2 and CO at the oxidation stage.

4. Conclusion

- A detailed four-step downdraft gasification process is modeled. Oxidation and reduction zones are modeled using the Gibbs free energy minimization approach. All chemical reactions reach equilibrium at the operating temperatures, respectively.
- The modeled process is validated with the experimental study conducted by Wei et al. on wood-fed gasifier. Simulation results showed an RMS error of 2.533.
- Parametric analysis was performed by varying gasifying agent composition, reduction zone temperature, equivalence ratio and, moisture content.
- The maximum value of cold gas efficiency (74%) was achieved at 750 ^{o}C. Thermal efficiency and low heating value at 750 ^{o}C were 84% and 5.66 MJ/Nm3, respectively. The main reaction controlling the H_2 yield was water gas reaction because of its endothermic nature.
- Cold gas and thermal efficiency reach to a maximum of 88 and 96%, respectively at ER = 0.14. Efficiencies continue to decrease with increase in moisture content.
- It is evident that for efficient gasification; operating temperature range of reduction zone should be 700-1000 ^{o}C, equivalence ratio between 0.1-0.2, and moisture content not exceeding 10%.
- Biochar production becomes zero when the gasification temperature reaches 700 ^{o}C and equivalence ratio becomes 0.14. The gasifier is to be operated below this temperature and equivalence ratio for the biochar production.

5. Acknowledgements

The authors would like to thank US Pakistan Center for Advanced Studies in Energy at NUST and the involved faculty and support staff for their pivotal contribution to this work.

Declaration of Interests: None

References

[1] Energy Information Administration U. International Energy Outlook 2013 with Projections to 2040. 2013.

[2] World Energy Outlook 2013 Factsheet. How will global energy markets evolve to 2035? 2013.

[3] Mathieu P, Dubuisson R. Performance analysis of a biomass gasifier. Energy Convers Manag 2002;43:1291–9. doi:10.1016/S0196-8904(02)00015-8.

[4] Bauen A, Berndes G, Junginger M, Londo M, Vuille F, Ball R, et al. Bioenergy: a sustainable and reliable energy source. A review of status and prospects. Bioenergy a Sustain Reliab Energy Source A Rev Status Prospect 2009.

[5] Basu P, Basu P. Introduction. Biomass Gasif Pyrolysis 2010:1–25. doi:10.1016/B978-0-12-374988-8.00001-5.

[6] Dincer I. Green methods for hydrogen production. Int J Hydrogen Energy 2012;37:1954–71. doi:10.1016/J.IJHYDENE.2011.03.173.

[7] Sharma S, Sheth PN. Air–steam biomass gasification: Experiments, modeling and simulation. Energy Convers Manag 2016;110:307–18. doi:10.1016/j.enconman.2015.12.030.

[8] Zhang L, Xu C (Charles), Champagne P. Overview of recent advances in thermo-chemical conversion of biomass. Energy Convers Manag 2010;51:969–82. doi:10.1016/J.ENCONMAN.2009.11.038.

[9] Bhavanam A, Sastry RC. Biomass Gasification Processes in Downdraft Fixed Bed Reactors : A Review. Int J Chem Eng Appl 2011;2:425–33. doi:10.1016/S0140-6701(98)96589-4.

[10] Lv P, Yuan Z, Wu C, Ma L, Chen Y, Tsubaki N. Bio-syngas production from biomass catalytic gasification. Energy Convers Manag 2007;48:1132–9. doi:10.1016/J.ENCONMAN.2006.10.014.
[11] Asadullah M, Ito S, Kunimori K, Yamada M, Tomishige K. Biomass Gasification to Hydrogen and Syngas at Low Temperature: Novel Catalytic System Using Fluidized-Bed Reactor. J Catal 2002;208:255–9. doi:10.1006/JCAT.2002.3575.
[12] Shen L, Gao Y, Xiao J. Simulation of hydrogen production from biomass gasification in interconnected fluidized beds. Biomass and Bioenergy 2008;32:120–7. doi:10.1016/J.BIOMBIOE.2007.08.002.
[13] Erkiaga A, Lopez G, Amutio M, Bilbao J, Olazar M. Influence of operating conditions on the steam gasification of biomass in a conical spouted bed reactor. Chem Eng J 2014;237:259–67. doi:10.1016/J.CEJ.2013.10.018.
[14] Dupont C, Boissonnet G, Seiler J-M, Gauthier P, Schweich D. Study about the kinetic processes of biomass steam gasification. Fuel 2007;86:32–40. doi:10.1016/J.FUEL.2006.06.011.
[15] Al Amoodi N, Kannan P, Al Shoaibi A, Srinivasakannan C. Aspen plus simulation of polyethylene gasification under equilibrium conditions. Chem Eng Commun 2013;200:977–92. doi:10.1080/00986445.2012.715108.
[16] Tremel A, Gaderer M, Spliethoff H. Small-scale production of synthetic natural gas by allothermal biomass gasification. Int J Energy Res 2013;37:1318–30. doi:10.1002/er.2933.
[17] Abdelouahed L, Authier O, Mauviel G, Corriou JP, Verdier G, Dufour A. Detailed Modeling of Biomass Gasification in Dual Fluidized Bed Reactors under Aspen Plus. Energy & Fuels 2012;26:3840–55. doi:10.1021/ef300411k.
[18] Kuo P-C, Wu W, Chen W-H. Gasification performances of raw and torrefied biomass in a downdraft fixed bed gasifier using thermodynamic analysis. Fuel 2014;117:1231–41. doi:10.1016/j.fuel.2013.07.125.
[19] Zheng H, Kaliyan N, Morey RV. Aspen Plus simulation of biomass integrated gasification combined cycle systems at corn ethanol plants. Biomass and Bioenergy 2013;56:197–210. doi:10.1016/j.biombioe.2013.04.032.
[20] De Kam MJ, Vance Morey R, Tiffany DG. Biomass Integrated Gasification Combined Cycle for heat and power at ethanol plants. Energy Convers Manag 2009;50:1682–90. doi:10.1016/j.enconman.2009.03.031.
[21] Begum S, Rasul MG, Akbar D, Ramzan N. Performance Analysis of an Integrated Fixed Bed Gasifier Model for Different Biomass Feedstocks 2013:6508–24. doi:10.3390/en6126508.
[22] Dejtrakulwong C, Patumsawad S. Four zones modeling of the downdraft biomass gasification process: Effects of moisture content and air to fuel ratio. Energy Procedia 2014;52:142–9. doi:10.1016/j.egypro.2014.07.064.
[23] Gagliano A, Nocera F, Bruno M, Cardillo G. Development of an Equilibrium-based Model of Gasification of Biomass by Aspen Plus. Energy Procedia 2017;111:1010–9. doi:10.1016/j.egypro.2017.03.264.
[24] Liu B. Comparative study of fluidized-bed and fixed-bed reactor for syngas methanation over Ni-W / TiO 2 -SiO 2 catalyst. J Energy Chem 2013;22:740–6. doi:10.1016/S2095-4956(13)60098-4.
[25] Qian K, Kumar A, Patil K, Bellmer D, Wang D, Yuan W, et al. Effects of Biomass Feedstocks and Gasification Conditions on the Physiochemical Properties of Char 2013:3972–86. doi:10.3390/en6083972.
[26] Wu Y, Yang W, Blasiak W. Energy and Exergy Analysis of High Temperature Agent Gasification of Biomass 2014:2107–22. doi:10.3390/en7042107.

[27] Bulmau C, Marculescu C, Badea A, Apostol T. Pyrolysis parameters influencing the bio-char generation from wooden biomass 2010;72.
[28] Rauch R, Hrbek J, Hofbauer H. Biomass gasification for synthesis gas production and applications of the syngas 2014;3. doi:10.1002/wene.97.
[29] Zhang J, Li W, Gan Z. Effect of supercritical water on the stability and activity of alkaline carbonate catalysts in coal gasification. J Energy Chem 2013;22:459–67. doi:10.1016/S2095-4956(13)60060-1.
[30] Molino A, Chianese S, Musmarra D. Biomass gasification technology: The state of the art overview. J Energy Chem 2016;25:10–25. doi:10.1016/j.jechem.2015.11.005.
[31] Chawdhury MA, Mahkamov K, Division IM, Sciences C, Road S. Development of a Small Downdraft Biomass Gasifier for Developing Countries 2011. doi:10.3329/jsr.v3i1.5613.
[32] Kumar A, Jones DD, Hanna MA. Thermochemical Biomass Gasification: A Review of the Current Status of the Technology 2009:556–81. doi:10.3390/en20300556.
[33] Srivastava T. Renewable Energy (Gasification). Adv Electron Electr Eng 2013;3:1243–50.
[34] Peng D, Robinson DB. A New Two-Constant Equation of State. Ind Eng Chem Fundam 1976;15:59–64. doi:10.1021/i160057a011.
[35] Aspen Technology I. Aspen Plus ® User Guide. Aspen Technol Inc 2000:936.
[36] Atnaw SM, Sulaiman SA, Yusup S. A Simulation Study of Downdraft Gasification of Oil-Palm Fronds using ASPEN PLUS. J Appl Sci 2011;11:1913–20. doi:10.3923/jas.2011.1913.1920.
[37] Sotudeh-Gharebaagh R, Legros R, Chaouki J, Paris J. Simulation of circulating fluidized bed reactors using ASPEN PLUS. Fuel 1998;77:327–37. doi:10.1016/S0016-2361(97)00211-1.
[38] Doherty W, Reynolds A, Kennedy D. Aspen Plus Simulation of Biomass Gasification in a Steam Blown Dual Fluidised Bed. Book/b Chapters 2013.
[39] Wei L, Thomasson JA, Bricka RM, Wooten J. Syn-Gas Quality Evaluation for Biomass Gasification with a Downdraft Gasifier 2013. doi:10.13031/2013.25938.
[40] Gagliano A, Nocera F, Patania F, Detommaso M, Bruno M. Evaluation of the performance of a small biomass gasifier and micro-CHP plant for agro-industrial firms. Int J Heat Technol 2015;33:145–54. doi:10.18280/ijht.330418.
[41] Gagliano A, Nocera F, Patania F, Bruno M, Castaldo DG. Comptes Rendus Chimie A robust numerical model for characterizing the syngas composition in a downdraft gasi fi cation process. Comptes Rendus - Chim 2016;19:441–9. doi:10.1016/j.crci.2015.09.019.
[42] Song G, Feng F, Xiao J, Shen L. Technical assessment of synthetic natural gas (SNG) production from agriculture residuals. J Therm Sci 2013;22:359–65. doi:10.1007/s11630-013-0636-8.
[43] Lu Y, Hu J, Han J, Yu F. Synthesis of gasoline-range hydrocarbons from nitrogen-rich syngas over a Mo/HZSM-5 bi-functional catalyst. J Energy Inst 2016;89:782–92. doi:10.1016/J.JOEI.2015.03.010.
[44] Somorin TO, Adesola S, Kolawole A. State-level assessment of the waste-to-energy potential (via incineration) of municipal solid wastes in Nigeria. J Clean Prod 2017;164:804–15. doi:10.1016/J.JCLEPRO.2017.06.228.
[45] Puig-arnavat M, Bruno JC, Coronas A. Modified Thermodynamic Equilibrium Model for Biomass Gasification : A Study of the Influence of Operating Conditions 2012. doi:10.1021/ef2019462.